HPC@UNM2005-001
January 2005

HPC@UNM
THE CENTER FOR HIGH PERFORMANCE COMPUTING

TECHNICAL REPORT

An Energy Consistent Material-Point Method for Dynamic Finite Deformation Plasticity

Authors

E. Love
The University of New Mexico
Department of Mathematics and Statistics

D. L. Sulsky
The University of New Mexico
Department of Mathematics and Statistics

The University of New Mexico
The Center for High Performance Computing
MSC01 1190 Albuquerque, NM 87131-001
505.277.8249 *(main)* 505.277.8235 *(fax)*
www.hpc.unm.edu

The University of New Mexico

Disclaimer

The Center for High Performance Computing (HPC@UNM)
provides a focus for high performance computing and communication at
the University of New Mexico (UNM). HPC@UNM is committed to innovative research
in computational and computer science with emphasis on both algorithm development
and application. As part of this commitment, HPC@UNM sponsors this technical report series.
The technical reports are subject to internal review by HPC@UNM. However, the material,
as presented, does not necessarily reflect any position of HPC@UNM. Further, neither UNM,
nor the HPC, makes any warranty or assumes any legal liability or responsibility for
the accuracy, completeness, or usefulness of any information contained in this report.

An Energy Consistent Material-Point Method for Dynamic Finite Deformation Plasticity

E. Love and D. L. Sulsky*

Department of Mathematics and Statistics, 415 Humanities Building,

MSC03 2150, University of New Mexico, Albuquerque, NM 87131-0001

January 11, 2005

Abstract

Energy consistency for the material-point method (MPM) is examined for thermodynamically consistent hyperelastic-plastic materials. It is shown that MPM can be formulated with implicit, three-field variational, finite element algorithms which dissipate energy and conserve momentum for that class of material models. With a consistent mass matrix the resulting overall numerical method inherits the energy dissipative and momentum conserving properties of the mesh solution. Thus the MPM algorithm proposed here satisfies by construction a time-discrete form of the second law of thermodynamics. Properties of the method are illustrated in numerical examples.

Keywords: Material-Point Method (MPM), Energy Consistency, Momentum Conservation, Finite Deformation Plasticity.

1 Introduction

The material-point method (MPM) is a general numerical tool for the mechanical analysis of continuous media [57], [59], [60]. This method utilizes two discretizations to solve the continuum equations describing the motion and deformation of fluids and solids. A Lagrangian description of the material under consideration is given by a set of unconnected material points that are tracked throughout the deformation. A background computational grid is used to calculate the interactions among the Lagrangian points through the solution of the momentum equation. A mapping between the two discretizations is performed at each step in the loading process. The constitutive equations are solved at each material point so that material models with history dependence are implemented easily. The method has proven to be particularly useful for problems displaying the large deformation that occurs with inelastic behavior of solids. The present work exploits developments in finite element analysis to construct an implicit energy and momentum consistent method for hyperelastic-plastic

*corresponding author. email: sulsky@math.unm.edu

solids, thus extending the work in [26], [30], [58]. Additionally, a three-field mixed formulation is considered, providing for a more general implementation than the two field mixed (MPM) formulation in [39].

Section 2 of this paper presents the continuum equations and reviews their conservation properties. The goal is to replicate these continuum properties in the discrete equations. Section 3 reviews the MPM computational cycle, including the integration of the plasticity equations, and examines conservation properties of the discretization. In order to have an energy-consistent method, the Lagrangian grid dynamics must dissipate energy and conserve momentum. For this step we make use of an implicit time integration scheme developed for the finite element method which has the desired properties. Thus, analysis of the grid dynamics follows [24], [35]. The MPM algorithm inherits the properties of the grid dynamics algorithm if a consistent mass matrix is used [14], [30].

Finally, in Section 4, numerical examples are presented that illustrate the properties of this energy consistent and momentum conserving material-point method. Section 5 closes the paper with some concluding remarks and observations.

2 The continuum problem

The goal of this section is to present the continuum equations of motion for a deformable solid body. These equations are well known, and the reader may consult the books [1], [16], [27], [34] or [41] for more information. After introducing the notation, the weak form of the linear momentum equation and the hyperelastic-plastic constitutive model are given. Next, conservation of linear momentum, angular momentum and energy are reviewed for the unforced, traction-free Neumann problem.

2.1 Basic notation

Let $\Omega_0 \in \mathbb{R}^3$ denote the reference (material) position of a continuum body, with material points labeled $\mathbf{X}$. The set Ω_0 is assumed open and bounded, with a smooth boundary Γ_0. Assume the reference boundary Γ_0 is partitioned into disjoint subsets such that $\Gamma_0 = \overline{\Gamma_{\boldsymbol{\varphi}} \bigcup \Gamma_{\boldsymbol{\sigma}}}$ and $\Gamma_{\boldsymbol{\varphi}} \bigcap \Gamma_{\boldsymbol{\sigma}} = \emptyset$.

Let the spatial (current) position of the same body be $\Omega \in \mathbb{R}^3$, with points labeled $\mathbf{x}$. Assume there exists a smooth mapping, the motion of the body, $\boldsymbol{\varphi} : \Omega_0 \times [0, \mathrm{T}] \to \mathbb{R}^3$, such that $\Omega = \boldsymbol{\varphi}(\Omega_0, \mathrm{t})$ and $\mathbf{x} = \boldsymbol{\varphi}(\mathbf{X}, \mathrm{t})$, where $[0, \mathrm{T}] \subset \mathbb{R}$ is the the time interval of interest. The deformation gradient of the motion is defined as

$$\mathbf{F}(\mathbf{X}, \mathrm{t}) := D\boldsymbol{\varphi} = \mathrm{GRAD}_{\mathbf{X}}[\boldsymbol{\varphi}]. \tag{1}$$

Given the above, the set of admissible configurations is then defined as

$$\mathcal{S} := \left\{ \boldsymbol{\varphi} : \Omega_0 \times [0, \mathrm{T}] \to \mathbb{R}^3 \mid J(\boldsymbol{\varphi}) := \det[\mathbf{F}] > 0 \text{ and } \boldsymbol{\varphi}|_{\Gamma_{\boldsymbol{\varphi}}} = \bar{\boldsymbol{\varphi}} \right\}, \tag{2}$$

where $\bar{\boldsymbol{\varphi}} : \Gamma_{\boldsymbol{\varphi}} \times [0, \mathrm{T}] \to \mathbb{R}^3$ is specified on $\Gamma_{\boldsymbol{\varphi}}$. The material velocity of a point $\mathbf{X}$ is defined as $\mathbf{v} := \dot{\boldsymbol{\varphi}}$, where the superposed dot denotes the material time derivative. Given a reference

density $\rho_0 : \Omega_0 \to \mathbb{R}^+$, the spatial density is $\rho = J^{-1}\rho_0$ and the material momentum is defined as $\boldsymbol{\pi} := \rho_0 \mathbf{v}$.

Let $\boldsymbol{\sigma}$ denote the Cauchy stress in the current configuration. The developments in this work critically use the *symmetric* Piola-Kirchhoff stress $\mathbf{S}$, defined such that

$$J\boldsymbol{\sigma} = \mathbf{F}\mathbf{S}\mathbf{F}^T. \tag{3}$$

The Kirchhoff stress is defined as

$$\boldsymbol{\tau} := \boldsymbol{\varphi}_*(\mathbf{S}) = \mathbf{F}\mathbf{S}\mathbf{F}^T, \tag{4}$$

with *deviatoric part* $\operatorname{dev}\boldsymbol{\tau} := \boldsymbol{\tau} - \frac{1}{3}\operatorname{trace}[\boldsymbol{\tau}]\,\mathbf{I}$, where $\boldsymbol{\varphi}_*(\cdot)$ denotes the standard push-forward operation [11], [34] of continuum mechanics and differential geometry, with corresponding pull back operation denoted by $\boldsymbol{\varphi}^*(\cdot)$. The prescribed traction boundary condition is

$$(\mathbf{F}\mathbf{S})\mathbf{N} = \bar{\mathbf{T}} \text{ on } \Gamma_{\boldsymbol{\sigma}}, \tag{5}$$

where $\mathbf{N} : \Gamma_0 \to S^2$ is the outward unit normal field to the material boundary Γ_0 and $\bar{\mathbf{T}} : \Gamma_{\boldsymbol{\sigma}} \times [0, \mathrm{T}] \to \mathbb{R}^3$ is the prescribed nominal traction vector. In addition to these boundary tractions, the body is assumed to be acted upon by a body force (per unit mass) $\mathbf{b} : \Omega_0 \times [0, \mathrm{T}] \to \mathbb{R}^3$.

2.2 Three field variational principle

Denote by $\mathcal{T}_{3\times3}$ the space of all rank two tensors. Let $\mathcal{T}^{sym}_{3\times3}$ be the subspace of all symmetric rank two tensors and $\mathcal{T}^{sym+}_{3\times3}$ be the convex subset of all symmetric, positive-definite rank two tensors. Let $\mathbf{C} := \mathbf{F}^T\mathbf{F}$ denote the right Cauchy-Green strain tensor and $\mathbf{b} := \mathbf{F}\mathbf{F}^T$ denote the left Cauchy-Green strain tensor. Notice that $\mathbf{C}$ and $\mathbf{b}$ have the same invariants and eigenvalues.

Initially, we shall assume that the body is isotropic and hyperelastic, so that at each material point $\mathbf{X} \in \Omega_0$ there exists an internal free energy of the form

$$W(\mathbf{C}) := \widehat{W}(\mathbf{C}) \; + \; U\left(\det(\mathbf{C})^{1/2}\right), \tag{6}$$

where $\widehat{W}$ is the deviatoric energy,

$$\widehat{W}(\lambda\mathbf{C}) = \widehat{W}(\mathbf{C}) \quad \forall\, \mathbf{C} \in \mathcal{T}^{sym+}_{3\times3} \text{ and } \forall \lambda \in \mathbb{R}^+, \tag{7}$$

and $U(J)$ is the volumetric energy. Under the assumption of isotropy, the energy function $\widehat{W}$ is a function only of the invariants of $\mathbf{C}$ (see the appendix of [27]), or equivalently only of the invariants of $\mathbf{b}$. Thus there exists a $\widetilde{W}(\mathbf{b})$ such that $\widehat{W}(\mathbf{C}) = \widetilde{W}(\mathbf{b})$, where isotropy (and invariance under superposed rigid body motions) requires that

$$\widetilde{W}(\mathbf{Q}\mathbf{b}\mathbf{Q}^T) = \widetilde{W}(\mathbf{b}) \quad \forall\, \mathbf{Q} \in SO(3). \tag{8}$$

Given isotropy, equation (6) may be written equivalently as a function of $\mathbf{b}$, so that

$$W(\mathbf{b}) := \widetilde{W}(\mathbf{b}) \; + \; U\left(\det(\mathbf{b})^{1/2}\right). \tag{9}$$

Denote by $\mathcal{W}$ the space of test functions associated with the admissible configurations in $\mathcal{S}$, defined in standard fashion as

$$\mathcal{W} := \left\{ \delta\boldsymbol{\varphi} : \Omega_0 \to \mathbb{R}^3 \mid \delta\boldsymbol{\varphi}|_{\Gamma_{\boldsymbol{\varphi}}} = \mathbf{0} \right\}. \tag{10}$$

It is convenient to introduce two inner product notations, $< \cdot, \cdot >_{\Omega_0}$ and $< \cdot, \cdot >_{\Gamma_0}$, denoting the L^2 inner product on Ω_0 and Γ_0, respectively, of scalars, vectors or tensors, depending on the context.

A three field variational statement [54], [55] of the equations of motion for a solid body can be derived from a Lagrangian of the form

$$\mathrm{L}(\boldsymbol{\varphi}, \mathbf{v}, \Theta, p) = \frac{1}{2}\langle \mathbf{v}, \rho_0 \mathbf{v} \rangle_{\Omega_0} - \int_{\Omega_0} \left[\widehat{W}(\mathbf{C}) + p(J(\mathbf{C}) - \Theta) + U(\Theta) \right] \mathrm{d}\Omega_0 - \Pi_{ext}(\boldsymbol{\varphi}), \tag{11}$$

for $\boldsymbol{\varphi} \in \mathcal{S}$, $\mathbf{v} \in \mathcal{W}$ and $p, \Theta \in L^2(\Omega_0)$. The variables $\{p, \Theta\}$ are the mixed pressure and the mixed volume, respectively. The external force potential function is

$$\Pi_{ext}(\boldsymbol{\varphi}) = \int_{\Omega_0} \pi_g(\boldsymbol{\varphi}) \mathrm{d}\Omega_0 \; + \; \int_{\Gamma_0} \pi_T(\boldsymbol{\varphi}) \mathrm{d}\Gamma_0, \tag{12}$$

where $\mathbf{b} = -\partial_{\boldsymbol{\varphi}} \pi_g$ and $\bar{\mathbf{T}} = -\partial_{\boldsymbol{\varphi}} \pi_T$.

The Euler-Lagrange equations associated with this Lagrangian are: find $\boldsymbol{\varphi} \in \mathcal{S}$ and $p, \Theta \in L^2(\Omega_0)$ such that

$$\langle \delta\boldsymbol{\varphi}, \dot{\boldsymbol{\pi}} \rangle_{\Omega_0} + \langle \mathrm{GRAD}_{\mathbf{X}}[\delta\boldsymbol{\varphi}], \mathbf{FS} \rangle_{\Omega_0} - \langle \delta\boldsymbol{\varphi}, \rho_0 \mathbf{b} \rangle_{\Omega_0} - \left\langle \delta\boldsymbol{\varphi}, \bar{\mathbf{T}} \right\rangle_{\Gamma_0} = 0 \tag{13a}$$

$$\langle \delta\Theta, p - \partial_\Theta U \rangle_{\Omega_0} = 0 \tag{13b}$$

$$\langle \delta p, J(\mathbf{C}) - \Theta \rangle_{\Omega_0} = 0, \tag{13c}$$

for all $\delta\boldsymbol{\varphi} \in \mathcal{W}$ and for all $\delta p, \delta\Theta \in L^2(\Omega_0)$, where

$$\left.\begin{aligned} \mathbf{S} &= 2\partial_{\mathbf{C}} \widehat{W} + 2p \left(\partial_{\mathbf{C}} J\right) \\ &= \boldsymbol{\varphi}^*(\operatorname{dev} \boldsymbol{\tau} + pJ\mathbf{I}) \end{aligned}\right\}, \tag{14}$$

and $2\partial_{\mathbf{C}} J = J\mathbf{C}^{-1}$.

Along with the above variational equation, the solution $\boldsymbol{\varphi}$ must also satisfy the initial conditions

$$\boldsymbol{\varphi}(\mathbf{X}, 0) = \boldsymbol{\varphi}_0 \;\text{ and }\; \boldsymbol{\pi}(\mathbf{X}, 0) = \rho_0 \mathbf{v}_0 \;\text{ in }\; \Omega_0. \tag{15}$$

Once a suitable constitutive equation relating $\mathbf{S}$ to the motion $\boldsymbol{\varphi}$ is specified, equations (13) and (15) together define a (generally) nonlinear initial boundary value problem for the motion $\boldsymbol{\varphi} \in \mathcal{S}$ of the body.

Remarks 2.1.

1. Although equations (13) have been derived as the Euler-Lagrange equations of a Lagrangian potential function, they are more generally applicable to non-conservative and dissipative dynamical processes. In this work they are used in the numerical simulation of plasticity.

2. The Lagrangian (11) is actually a simplified version of the more general Lagrangian

$$\mathrm{L}(\boldsymbol{\varphi}, \mathbf{v}, \Theta, p) = \frac{1}{2}\langle \mathbf{v}, \rho_0 \mathbf{v}\rangle_{\Omega_0} - \int_{\Omega_0} \left\{ W\left((\Theta/J)^{1/3}\mathbf{C}\right) + p(J-\Theta)\right\} \mathrm{d}\Omega_0 - \Pi_{ext}(\boldsymbol{\varphi}),$$

where no a-priori assumptions about the character of the free energy W are made [24],[54],[55],[66]. However, under the conditions of equation (6), this more general expression collapses to the form in (11), which is both simpler to implement and sufficient for the purposes of this work.

3. An augmented Lagrangian algorithm [22], [24], [54] can be applied within this three-field mixed framework to enforce the incompressibility constraint $\Theta = 1$. Reference [39] considers a two-field $\{\boldsymbol{\varphi}, p\}$ formulation for incompressibility within an MPM context.

2.3 Isotropic multiplicative plasticity

Isotropic finite strain multiplicative plasticity with isotropic hardening has the following set of assumptions [49],[50],[52]:

1. There exists a convex elastic domain

$$\mathbb{E} := \left\{ (\boldsymbol{\tau}, q) \in \mathcal{T}^{sym}_{3\times 3} \times \mathbb{R} \mid \Phi(\boldsymbol{\tau}, q) \leq 0 \right\}, \tag{16}$$

where q is a scalar stress-like isotropic hardening variable and Φ is the (smooth) yield function. Invariance under superposed rigid body motions requires Φ to be an isotropic function of the stress,

$$\Phi(\mathbf{Q}\boldsymbol{\tau}\mathbf{Q}^T, q) = \Phi(\boldsymbol{\tau}, q) \quad \forall\, \mathbf{Q} \in SO(3). \tag{17}$$

2. The deformation gradient admits a multiplicative decomposition into elastic and plastic parts [6], [29] such that

$$\mathbf{F} = \mathbf{F}^e\mathbf{F}^p. \tag{18}$$

Consistent with this define $J^e := \det \mathbf{F}^e$ and $J^p := \det \mathbf{F}^p$ so that $J = J^eJ^p$. All developments herein are based upon the elastic left Cauchy-Green strain tensor

$$\mathbf{b}^e := \mathbf{F}^e\mathbf{F}^{eT}, \tag{19}$$

and the inverse plastic metric

$$\mathbf{G}^p := \left[\mathbf{F}^{pT}\mathbf{F}^p\right]^{-1}, \tag{20}$$

where

$$\mathbf{b}^e = \mathbf{F}\mathbf{G}^p\mathbf{F}^T. \tag{21}$$

3. The stress response of the material is given by an internal free energy function $W(\mathbf{b}^e, \xi)$, where $\xi \geq 0$ is a scalar strain-like isotropic hardening variable. The stress-like hardening variable q is conjugate to ξ in the sense that

$$q := -\partial_\xi W. \tag{22}$$

Invariance requires that the free energy function W be isotropic in the sense that

$$W(\mathbf{Q}\mathbf{b}^e\mathbf{Q}^T, \xi) = W(\mathbf{b}^e, \xi) \quad \forall\, \mathbf{Q} \in SO(3). \tag{23}$$

2.3.1 Dissipation inequality

The starting point for the derivation of the constitutive equations is a reduced form of the second law of thermodynamics. At every material point $\mathbf{X} \in \Omega_0$ the internal dissipation is defined as

$$\left.\begin{aligned} \mathcal{D}^{int} &:= \boldsymbol{\tau} : \mathbf{d} - \frac{\mathrm{d}}{\mathrm{dt}} W(\mathbf{b}^e, \xi) \geq 0 \\ &= \frac{1}{2}\mathbf{S} : \dot{\mathbf{C}} - \frac{\mathrm{d}}{\mathrm{dt}} W(\mathbf{b}^e, \xi) \geq 0 \end{aligned}\right\}, \tag{24}$$

where the rate of deformation tensor is $\mathbf{d} = \mathrm{sym}(\mathbf{l}) = \mathrm{sym}(\dot{\mathbf{F}}\mathbf{F}^{-1}) = \frac{1}{2}\boldsymbol{\varphi}_*(\dot{\mathbf{C}})$. Defining

$$\mathcal{L}_v \mathbf{b}^e := \mathbf{F}\left[\frac{\mathrm{d}}{\mathrm{dt}}\mathbf{G}^p\right]\mathbf{F}^T \tag{25}$$

as the Lie derivative of $\mathbf{b}^e$, and noting that equation (21) implies

$$\dot{\mathbf{b}}^e = \mathbf{l}\mathbf{b}^e + \mathbf{b}^e\mathbf{l}^T + \mathcal{L}_v\mathbf{b}^e, \tag{26}$$

one may show

$$\begin{aligned} \frac{\mathrm{d}}{\mathrm{dt}} W &= \partial_{\mathbf{b}^e} W : (\mathbf{l}\mathbf{b}^e + \mathbf{b}^e\mathbf{l}^T + \mathcal{L}_v\mathbf{b}^e) + (\partial_\xi W)\dot{\xi} \\ &= \partial_{\mathbf{b}^e} W : (\mathbf{l}\mathbf{b}^e + \mathbf{b}^e\mathbf{l}^T) + \partial_{\mathbf{b}^e} W : \mathcal{L}_v\mathbf{b}^e - q\dot{\xi} \\ &= (2\mathbf{b}^e\partial_{\mathbf{b}^e} W) : \mathbf{l} \;+\; \partial_{\mathbf{b}^e} W : \mathcal{L}_v\mathbf{b}^e - q\dot{\xi} \\ &= (2\mathbf{b}^e\partial_{\mathbf{b}^e} W) : \mathbf{d} \;+\; [2\mathbf{b}^e\partial_{\mathbf{b}^e} W] : \left[\frac{1}{2}(\mathcal{L}_v\mathbf{b}^e)\mathbf{b}^{e-1}\right] - q\dot{\xi}. \end{aligned} \tag{27}$$

Two facts have been used above. First, as a consequence of isotropy, $\mathbf{b}^e$ and $\partial_{\mathbf{b}^e} W$ commute, and second $\mathbf{b}^e(\partial_{\mathbf{b}^e} W)$ is symmetric. Thus the dissipation inequality (24) may be rewritten as

$$\mathcal{D}^{int} = [\boldsymbol{\tau} - 2\mathbf{b}^e\partial_{\mathbf{b}^e} W] : \mathbf{d} + [2\mathbf{b}^e\partial_{\mathbf{b}^e} W] : \left[-\frac{1}{2}(\mathcal{L}_v\mathbf{b}^e)\mathbf{b}^{e-1}\right] + q\dot{\xi} \geq 0. \tag{28}$$

Definition 2.1. *Coleman-Noll Entropy Principle* [1]. The constitutive functions must satisfy the dissipation inequality for all thermomechanical processes. Thus, by varying the process, one may vary $\mathbf{d}$ *independently* of $\{(\mathcal{L}_v\mathbf{b}^e), \dot{\xi}\}$ at $\{\mathbf{X}, \mathrm{t}\}$.

The Coleman-Noll Entropy Principle subsequently implies that

$$\boxed{\boldsymbol{\tau} = 2\mathbf{b}^e(\partial_{\mathbf{b}^e} W) = 2(\partial_{\mathbf{b}^e} W)\mathbf{b}^e} \tag{29}$$

and

$$\mathcal{D}^{int} = \boldsymbol{\tau} : \left[-\frac{1}{2}(\mathcal{L}_v\mathbf{b}^e)\mathbf{b}^{e-1}\right] + q\dot{\xi} \geq 0. \tag{30}$$

Many authors at this juncture adopt the postulate of maximum dissipation [31], [49], [50], [52] to derive the flow rules for the plastic internal variables. However, we simply propose *associative* flow rules, consistent with the developments of the small strain theory [51], as

$$-\frac{1}{2}(\mathcal{L}_v\mathbf{b}^e) = \dot{\gamma}\,[\partial_{\boldsymbol{\tau}}\Phi]\,\mathbf{b}^e, \tag{31a}$$

$$\boxed{\dot{\xi} = \dot{\gamma}\, \partial_q \Phi,} \tag{31b}$$

for a plastic consistency parameter $\dot{\gamma} \geq 0$. This reduces the internal dissipation to

$$\mathcal{D}^{int} = \dot{\gamma}\, [(\boldsymbol{\tau} : \partial_{\boldsymbol{\tau}} \Phi) + (q \cdot \partial_q \Phi)] \geq 0. \tag{32}$$

Since the elastic domain $\mathbb{E} \subset \mathbb{R}^7$ is a convex set containing the origin, $[(\boldsymbol{\tau} : \partial_{\boldsymbol{\tau}} \Phi) + (q \cdot \partial_q \Phi)] \geq 0$, and *the dissipation inequality is satisfied by construction.* Using equations (21) and (25) the flow rule (31a) has the equivalent form

$$\boxed{\dot{\mathbf{G}}^p = -2\dot{\gamma} \left(\mathbf{F}^{-1} [\partial_{\boldsymbol{\tau}} \Phi]\, \mathbf{F}\right) \mathbf{G}^p.} \tag{33}$$

The plastic consistency parameter $\dot{\gamma}$ remains to be defined. The two cases of interest are:

1. *Rate independent plasticity.* In this case $\dot{\gamma}$ is the Lagrange multiplier associated with the inequality constraint $\Phi \leq 0$ and is given by the Kuhn-Tucker conditions

$$\dot{\gamma} \geq 0, \quad \Phi \leq 0, \quad \dot{\gamma}\Phi = 0. \tag{34}$$

2. *Viscoplasticity.* In this case $\dot{\gamma}$ is given by a viscoplastic regularization

$$\dot{\gamma} = \frac{< \Phi >}{\eta}, \tag{35}$$

where $\eta > 0$ is the viscosity parameter. The Macauley bracket function is

$$< x > \; = \; \frac{1}{2}(x + |x|). \tag{36}$$

In the limit as $\eta \searrow 0$ the rate independent case is recovered.

2.3.2 J^2 flow model

For the purposes of this work, and without loss of generality, a J^2 flow model of plasticity is considered. The model is as follows:

- The yield function takes the simple form

$$\Phi(\boldsymbol{\tau}, q) := \| \operatorname{dev} \boldsymbol{\tau} \| - \sqrt{\frac{2}{3}}(\sigma_Y - q), \tag{37}$$

where $\sigma_Y \geq 0$ is the flow (yield) stress. In this case

$$\mathbf{n} := \partial_{\boldsymbol{\tau}} \Phi = \frac{\operatorname{dev} \boldsymbol{\tau}}{\| \operatorname{dev} \boldsymbol{\tau} \|}, \tag{38}$$

and

$$\partial_q \Phi = \sqrt{\frac{2}{3}}, \tag{39}$$

so that

$$\dot{\mathbf{G}}^p = -2\dot{\gamma}\left(\mathbf{F}^{-1}\mathbf{n}\,\mathbf{F}\right)\mathbf{G}^p, \tag{40}$$

and

$$\dot{\xi} = \dot{\gamma}\sqrt{\frac{2}{3}}. \tag{41}$$

The internal dissipation (32) simplifies to

$$\mathcal{D}^{int} = \dot{\gamma}\left[\|\operatorname{dev}\boldsymbol{\tau}\| + q\sqrt{\frac{2}{3}}\right] = \dot{\gamma}\left[\Phi + \sqrt{\frac{2}{3}}(\sigma_Y - q) + q\sqrt{\frac{2}{3}}\right] = \dot{\gamma}\left[\Phi + \sqrt{\frac{2}{3}}\sigma_Y\right]. \tag{42}$$

For this classical model of plasticity, the hardening parameter ξ is often termed the *equivalent plastic strain*.

- Let $\boldsymbol{\varepsilon}^e = \operatorname{diag}\{\varepsilon_1^e, \varepsilon_2^e, \varepsilon_3^e\}$ be the vector of principal elastic stretches, the eigenvalues of $\sqrt{\mathbf{b}^e}$. Let $\boldsymbol{\beta} = \operatorname{diag}\{\beta_1, \beta_2, \beta_3\}$ be the vector of principal Kirchhoff stresses, the eigenvalues of $\boldsymbol{\tau}$. For isotropic models one can use the chain rule to show that $\beta_A = \partial_{\varepsilon_A^e} W$ [65]. The elastic response is given by

$$W(\mathbf{b}^e, \xi) = G\|\operatorname{dev}\boldsymbol{\varepsilon}^e\|^2 + U(J^e) + \mathcal{H}(\xi), \tag{43}$$

where $G \geq 0$ is the (linearized) elastic shear modulus. This is often referred to as the Hencky model of finite strain elasticity [50], [65]. Notice that this free energy function satisfies the assumption of equations (6) and (9) so that

$$\widetilde{W}(\mathbf{b}^e, \xi) = G\|\operatorname{dev}\boldsymbol{\varepsilon}^e\|^2 + \mathcal{H}(\xi) \quad \Longrightarrow \quad \operatorname{dev}\boldsymbol{\tau} = 2(\partial_{\mathbf{b}^e}\widetilde{W})\mathbf{b}^e. \tag{44}$$

For the Hencky model the principal values of $\operatorname{dev}\boldsymbol{\tau}$ are $\boldsymbol{\beta} = \partial_{\boldsymbol{\varepsilon}^e}\widetilde{W} = 2G\operatorname{dev}\boldsymbol{\varepsilon}^e$. Finally, for linear isotropic hardening

$$\mathcal{H}(\xi) := \frac{1}{2}H\xi^2, \tag{45}$$

with the hardening parameter $H \geq 0$, so that $q = -H\xi$.

Remarks 2.2.

1. Unfortunately, the Hencky model of finite strain elasticity is not polyconvex [49], [50]. Thus it is not appropriate for use when large elastic strains are present, and in fact numerical difficulties have been encountered [44]. However, the model very much simplifies the numerical implementation of the plasticity equations and provides a valid approximation for small to moderate elastic strains. For typical metal plasticity the elastic strains are small relative to the plastic strains, and the Hencky model is suitable.

2. It is not strictly necessary to assume that the yield function is based upon the Kirchhoff stresses $\boldsymbol{\tau}$. The equations can be formulated assuming that the Cauchy stresses $\boldsymbol{\sigma}$ determine the yield criterion, and one might argue this to be more physically correct. In such a situation the flow rules are by necessity non-associative, even with the postulate of maximum plastic dissipation [37]. For this presentation it is sufficient to consider the plasticity equations as presented above, with the knowledge that a modification to the constitutive model is not difficult.

2.4 Conservation properties

The evolutionary equations (13) possess a number of important global conservation properties. First, linear momentum, angular momentum, and total energy, are defined. Next, it is shown that (13) conserves momentum and dissipates total energy under appropriate conditions on the loading and boundary conditions.

Definition 2.2. The *total linear momentum* $\mathbf{L}$ is defined as

$$\mathbf{L} := \int_{\Omega_0} \boldsymbol{\pi} \, \mathrm{d}\Omega_0. \tag{46}$$

Definition 2.3. The *total angular momentum* $\mathbf{J}$ is defined as

$$\mathbf{J} := \int_{\Omega_0} (\boldsymbol{\varphi} \times \boldsymbol{\pi}) \, \mathrm{d}\Omega_0. \tag{47}$$

Definition 2.4. The *total kinetic energy* T is defined as

$$2\mathsf{T} := \left\langle \boldsymbol{\pi}, \rho_0^{-1}\boldsymbol{\pi} \right\rangle_{\Omega_0} = \left\langle \boldsymbol{\pi}, \mathbf{v} \right\rangle_{\Omega_0} = \left\langle \rho_0 \mathbf{v}, \mathbf{v} \right\rangle_{\Omega_0}. \tag{48}$$

Definition 2.5. The *total potential energy* V is defined as

$$\mathsf{V} := \int_{\Omega_0} \left[\widetilde{W}(\mathbf{b}^e, \xi) + U(\Theta) \right] \, \mathrm{d}\Omega_0. \tag{49}$$

Definition 2.6. The *total energy* H is defined as

$$\mathsf{H} := \mathsf{T} + \mathsf{V}. \tag{50}$$

Theorem 2.1. Let $\Gamma_{\boldsymbol{\varphi}} = \emptyset$, $\mathbf{b} = \mathbf{0}$ and $\bar{\mathbf{T}} = \mathbf{0}$. Then total linear momentum $\mathbf{L}$ and the total angular momentum $\mathbf{J}$ are constants of the motion, and the total energy H is dissipated.

Proof. This result is well known, and is based on classical arguments.

1. *Linear Momentum is conserved.* See [30].
2. *Angular Momentum is conserved.* Conservation of angular momentum is a direct result of the symmetry of the stress tensor $\mathbf{S}$ [30].
3. *Energy is dissipated.* Consider variations of the form

$$\delta\boldsymbol{\varphi}(\mathbf{X}) = \mathbf{v}, \quad \delta p(\mathbf{X}) = 1, \quad \delta\Theta(\mathbf{X}) = 1, \tag{51}$$

which are admissible when $\Gamma_{\boldsymbol{\varphi}} = \emptyset$ (or when $\bar{\boldsymbol{\varphi}} = \mathbf{0}$). This choice shows that the time rate of change of the total energy is negative,

$$\begin{aligned}
\frac{\mathrm{d}}{\mathrm{dt}}\mathsf{H} &= \frac{\mathrm{d}}{\mathrm{dt}}\mathsf{T} + \frac{\mathrm{d}}{\mathrm{dt}}\mathsf{V} \\
&= \langle \mathbf{v}, \dot{\boldsymbol{\pi}} \rangle_{\Omega_0} + \int_{\Omega_0} \left[\dot{\widetilde{W}}(\mathbf{b}^e, \xi) + \dot{U}(\Theta) \right] \, \mathrm{d}\Omega_0 \\
&= \langle \mathbf{v}, \dot{\boldsymbol{\pi}} \rangle_{\Omega_0} + \int_{\Omega_0} \left[\mathrm{dev}\, \boldsymbol{\tau} : \mathbf{d} - \mathcal{D}^{int} + U'(\Theta)\dot{\Theta} \right] \, \mathrm{d}\Omega_0 \quad \text{(by(24))} \\
&= \langle \mathbf{v}, \dot{\boldsymbol{\pi}} \rangle_{\Omega_0} + \int_{\Omega_0} \left[\mathrm{dev}\, \boldsymbol{\tau} : \mathbf{d} - \mathcal{D}^{int} + p\dot{\Theta} \right] \, \mathrm{d}\Omega_0 \\
&= \langle \mathbf{v}, \dot{\boldsymbol{\pi}} \rangle_{\Omega_0} + \int_{\Omega_0} \left[\mathrm{dev}\, \boldsymbol{\tau} : \mathbf{d} + p\dot{J} - \mathcal{D}^{int} \right] \, \mathrm{d}\Omega_0 \\
&= \langle \mathbf{v}, \dot{\boldsymbol{\pi}} \rangle_{\Omega_0} + \int_{\Omega_0} \left[\frac{1}{2}\boldsymbol{\varphi}^*(\mathrm{dev}\, \boldsymbol{\tau}) : \dot{\mathbf{C}} + p(\partial_{\mathbf{C}} J) : \dot{\mathbf{C}} - \mathcal{D}^{int} \right] \, \mathrm{d}\Omega_0 \\
&= \langle \mathbf{v}, \dot{\boldsymbol{\pi}} \rangle_{\Omega_0} + \int_{\Omega_0} \left[[\boldsymbol{\varphi}^*(\mathrm{dev}\, \boldsymbol{\tau}) + 2p(\partial_{\mathbf{C}} J)] : \mathbf{F}^T\dot{\mathbf{F}} - \mathcal{D}^{int} \right] \, \mathrm{d}\Omega_0 \\
&= \langle \mathbf{v}, \dot{\boldsymbol{\pi}} \rangle_{\Omega_0} + \int_{\Omega_0} \left[\mathbf{FS} : \mathrm{GRAD}_{\mathbf{X}}[\mathbf{v}] - \mathcal{D}^{int} \right] \, \mathrm{d}\Omega_0 \\
&= \langle \mathbf{v}, \dot{\boldsymbol{\pi}} \rangle_{\Omega_0} + \langle \mathrm{GRAD}_{\mathbf{X}}[\mathbf{v}], \mathbf{FS} \rangle_{\Omega_0} - \int_{\Omega_0} \mathcal{D}^{int} \, \mathrm{d}\Omega_0 \\
&= -\int_{\Omega_0} \mathcal{D}^{int} \, \mathrm{d}\Omega_0 \\
&\leq 0. \qquad (52)
\end{aligned}$$

□

The goal of this work is to construct a discrete material-point method (MPM) which also satisfies these conservation properties.

3 The Material Point Method

The purpose of this section is to describe the material-point method (MPM) for the problem of equation (13). After introducing notation used to describe the discrete solution, the main steps in the MPM algorithm are presented. These are the numerical integration of the plasticity equations, discrete derivatives and the time stepping algorithm. The conservation properties of the MPM algorithm are also examined.

3.1 Basic notation

MPM consists of a set of material points and a background grid or mesh. Let $N_{pt} > 0$ denote the number of material points of the discrete simulation, and let $N_{nodes} > 0$ denote the number of nodes of the background mesh. Any quantity associated with a material

point is identified by a superscript $(\cdot)^{pt}$. For example, the velocity of a material point is notated as $\mathbf{v}^{pt}$. Any quantity associated with the background mesh is identified by a superscript $(\cdot)^h$, with $h > 0$ denoting the mesh size, or by indexes $\{A, B, C \dots\}$ indicating nodal values. For example, $\mathbf{v}^h(\mathbf{x})$ is the velocity field of the mesh with nodal values $\mathbf{v}_A$ for $A \in \{1, 2, \dots, N_{nodes}\}$. (In a slight abuse of notation, $(\cdot)^h$ is also used to notate the vector of nodal values of $(\cdot)$. This should not cause the reader any confusion in the context where it is used.) A subscript $(\cdot)_{n+1}$ indicates the time step index, corresponding to a solution at time t_{n+1}. A capital Δ is used to indicate a time step increment in a quantity, $\Delta(\cdot) = (\cdot)_{n+1} - (\cdot)_n$, and in standard fashion, $(\cdot)_{n+\alpha} := (1-\alpha)(\cdot)_n + \alpha(\cdot)_{n+1}\ \forall \alpha \in [0,1]$.

3.2 Numerical integration of plasticity equations

Let $\Delta \mathrm{t} > 0$ be the numerical time step. The goal is to discretely integrate the plasticity evolution equations, producing stresses and internal variables at time t_{n+1} from the initial conditions at time t_n. The numerical implementation involves an operator splitting procedure.

3.2.1 Predictor-Corrector algorithm

The first step in an operator split approach is the solution of the predictor phase. Assuming no plastic behavior, the flow rules reduce to

$$\dot{\mathbf{G}}^p = \mathbf{0} \quad \text{and} \quad \dot{\xi} = 0. \tag{53}$$

The solution to these equations are simply

$$\mathbf{G}^{p^{tr}}_{n+1} = \mathbf{G}^p_n \quad \text{and} \quad \xi^{tr}_{n+1} = \xi_n, \tag{54}$$

where the superscript "tr" indicates that these are the trial values of the plastic internal variables at time t_{n+1}. Define the trial stress as

$$\boldsymbol{\tau}^{tr}_{n+1} := 2\mathbf{b}^{e^{tr}}_{n+1} \partial_{\mathbf{b}^e} W(\mathbf{b}^{e^{tr}}_{n+1}, \xi^{tr}_{n+1}), \tag{55}$$

the trial hardening variable as

$$q^{tr}_{n+1} := -\partial_\xi W(\mathbf{b}^{e^{tr}}_{n+1}, \xi^{tr}_{n+1}), \tag{56}$$

and the trial value of the yield function as $\Phi^{tr}_{n+1} := \Phi(\boldsymbol{\tau}^{tr}_{n+1}, q^{tr}_{n+1})$. By checking the value of the yield function, the next step is determined :

$$\left.\begin{array}{l} \Phi^{tr}_{n+1} < 0 \implies \text{elastic step} \\ \Phi^{tr}_{n+1} > 0 \implies \text{plastic step} \end{array}\right\}.$$

If $\Phi^{tr}_{n+1} < 0$, simply set

$$\boldsymbol{\tau}_{n+1} = \boldsymbol{\tau}^{tr}_{n+1}, \quad \mathbf{G}^p_{n+1} = \mathbf{G}^p_n, \quad \xi_{n+1} = \xi_n.$$

If $\Phi^{tr}_{n+1} > 0$, the trial state is invalid and must be corrected.

The plastic corrector step is conducted by solving the equations

$$\dot{\mathbf{G}}^p = -2\dot{\gamma}\,\left(\mathbf{F}^{-1}\mathbf{n}\mathbf{F}\right)\mathbf{G}^p \tag{57}$$

and

$$\dot{\xi} = \dot{\gamma}\partial_q\Phi, \tag{58}$$

along with the yield condition

$$\dot{\gamma} = \frac{\Phi_{n+1}}{\eta}. \tag{59}$$

Motivated by the developments in [17],[49],[50] and [62] a backward Euler exponential update in time produces the equation

$$\begin{aligned}\mathbf{G}^p_{n+1} &= \exp\left(-2\dot{\gamma}_{n+1}\Delta\mathrm{t}\mathbf{F}^{-1}_{n+1}\mathbf{n}_{n+1}\mathbf{F}_{n+1}\right)\mathbf{G}^{p^{tr}}_{n+1}\\ &= \mathbf{F}^{-1}_{n+1}\exp(-2\Delta\gamma\mathbf{n}_{n+1})\mathbf{F}_{n+1}\,\mathbf{G}^{p^{tr}}_{n+1},\end{aligned} \tag{60}$$

where $\Delta\gamma := \dot{\gamma}_{n+1}\Delta\mathrm{t}$. Given that $\mathbf{b}^e_{n+1} = \mathbf{F}_{n+1}\mathbf{G}^p_{n+1}\mathbf{F}^T_{n+1}$, this may be written as

$$\mathbf{b}^e_{n+1} = \exp(-2\Delta\gamma\mathbf{n}_{n+1})\mathbf{b}^{e^{tr}}_{n+1}, \tag{61}$$

where $\mathbf{b}^{e^{tr}}_{n+1} = \mathbf{F}_{n+1}\mathbf{G}^{p^{tr}}_{n+1}\mathbf{F}^T_{n+1}$. A backward Euler time discretization of the flow rule for ξ yields

$$\xi_{n+1} - \xi^{tr}_{n+1} = \Delta\gamma\cdot\partial_q\Phi_{n+1} \tag{62}$$

and for the consistency condition is

$$\Delta\gamma = \Phi_{n+1}\frac{\Delta\mathrm{t}}{\eta}. \tag{63}$$

Let $\{\left(\lambda^{e^{tr}}_A\right)^2, \mathbf{m}^{tr}_A\}$ be the eigenpairs of $\mathbf{b}^{e^{tr}}_{n+1}$, let $\{(\lambda^e_A)^2, \mathbf{m}_A\}$ be the eigenpairs of $\mathbf{b}^e_{n+1}$ and let β_A be the eigenvalues of $\boldsymbol{\tau}_{n+1}$. Consistent with the assumption of isotropy, the spectral decompositions

$$\mathbf{b}^{e^{tr}}_{n+1} = \sum_{A=1}^{3}\left(\lambda^{e^{tr}}_A\right)^2\mathbf{m}^{tr}_A\otimes\mathbf{m}^{tr}_A, \tag{64}$$

$$\mathbf{b}^e_{n+1} = \sum_{A=1}^{3}\left(\lambda^e_A\right)^2\mathbf{m}_A\otimes\mathbf{m}_A, \tag{65}$$

$$\boldsymbol{\tau}_{n+1} = \sum_{A=1}^{3}\beta_A\,\mathbf{m}_A\otimes\mathbf{m}_A \tag{66}$$

and

$$\mathbf{n}_{n+1} = \sum_{A=1}^{3}(\partial_{\beta_A}\Phi_{n+1})\,\mathbf{m}_A\otimes\mathbf{m}_A \tag{67}$$

are valid. The fact that Φ is an isotropic function of $\boldsymbol{\tau}$ has been used. The isotropy assumption restricts Φ to be a function of the invariants of $\boldsymbol{\tau}$ and hence the derivative $\mathbf{n} = \partial_{\boldsymbol{\tau}}\Phi$ and $\boldsymbol{\tau}$ are coaxial. Now, inverting equation (61) produces

$$\mathbf{b}^{e^{tr}}_{n+1} = \exp\left(+2\Delta\gamma\mathbf{n}_{n+1}\right)\mathbf{b}^e_{n+1}, \tag{68}$$

which reduces to

$$\sum_{A=1}^{3}\left(\lambda_A^{e^{tr}}\right)^2 \mathbf{m}_A^{tr}\otimes\mathbf{m}_A^{tr} \quad = \quad \sum_{A=1}^{3}\exp\left[2\Delta\gamma(\partial_{\beta_A}\Phi_{n+1})\right](\lambda_A^e)^2\,\mathbf{m}_A\otimes\mathbf{m}_A. \tag{69}$$

A solution to the above equation is

$$\mathbf{m}_A = \mathbf{m}_A^{tr} \quad \text{and} \quad \exp\left[2\Delta\gamma(\partial_{\beta_A}\Phi_{n+1})\right](\lambda_A^e)^2 = \left(\lambda_A^{e^{tr}}\right)^2. \tag{70}$$

Let $\epsilon_A^e := \log(\lambda_A^e)$ and $\epsilon_A^{e^{tr}} := \log(\lambda_A^{e^{tr}})$. Then, taking the natural logarithm of both sides of the above equation and rearranging terms generates

$$\epsilon_A^e = \epsilon_A^{e^{tr}} - \Delta\gamma\cdot(\partial_{\beta_A}\Phi_{n+1}). \tag{71}$$

Note that this equation has the identical structure of a small strain, backward-Euler plasticity update [51]. Thus the plasticity update equations reduce to a (generally nonlinear) set of algebraic equations in principal stress-strain space [44]:

$$\boxed{\begin{aligned}\epsilon_A^e - \epsilon_A^{e^{tr}} + \Delta\gamma\cdot(\partial_{\beta_A}\Phi_{n+1}) &= 0\\ \beta_A - \partial_{\epsilon_A^e}W_{n+1} &= 0\\ \xi_{n+1} - \xi_{n+1}^{tr} - \Delta\gamma\cdot\partial_q\Phi_{n+1} &= 0\\ \Phi_{n+1} - \frac{\eta}{\Delta \mathrm{t}}\Delta\gamma &= 0\end{aligned}} \quad \text{for} \quad A=\{1,2,3\}. \tag{72}$$

Notice that these equations are well defined in the limit as $\eta \searrow 0$. For the J^2 plasticity model of section 2.3.2, the set of equations is linear with a closed form solution

$$\Delta\gamma = \left[\frac{\eta}{\Delta \mathrm{t}} + \frac{2}{3}H + 2G\right]^{-1}\Phi_{n+1}^{tr}. \tag{73}$$

Remarks 3.1. Any convenient method can be used to diagonalize $\mathbf{b}_{n+1}^{e^{tr}}$. Since this tensor (matrix) is small and symmetric there are a number of reliable and accurate numerical algorithms available [43].

3.2.2 Algorithmic dissipation

Assuming plastic flow and using equation (42), a discrete backward Euler approximation to the internal dissipation is

$$\begin{aligned}\Delta\mathcal{D}^{int} &:= \int_{\mathrm{t}_n}^{\mathrm{t}_{n+1}}\mathcal{D}^{int}\,\mathrm{dt}\\ &= \int_{\mathrm{t}_n}^{\mathrm{t}_{n+1}}\dot\gamma\left[\Phi + \sqrt{\frac{2}{3}}\sigma_Y\right]\,\mathrm{dt}\\ &\approx \left[\Phi_{n+1} + \sqrt{\frac{2}{3}}\sigma_Y\right]\Delta\gamma\\ &= \left[\frac{\eta}{\Delta \mathrm{t}}\Delta\gamma + \sqrt{\frac{2}{3}}\sigma_Y\right]\Delta\gamma\\ &\geq 0.\end{aligned} \tag{74}$$

Notice that this approximation is well defined as $\eta \searrow 0$. When there is no plastic flow $\Delta\mathcal{D}^{int} = 0$. For more general plasticity models, equation (32), for example, can be used to derive expressions for the algorithmic dissipation.

3.3 Discrete derivatives

Definition 3.1. *Discrete Derivative* [25]. Let $\mathbb{K} \subset \mathbb{R}^n$ be a convex set and assume there exists a smooth function $f : \mathbb{K} \to \mathbb{R}$. A *discrete derivative* $\mathrm{D}_{\mathbf{z}} f : \mathbb{K} \times \mathbb{K} \to \mathbb{R}^n$ is a mapping such that

1. Directionality.
$$\mathrm{D}_{\mathbf{z}} f(\mathbf{z}_1, \mathbf{z_2}) \cdot (\mathbf{z}_2 - \mathbf{z}_1) = f(\mathbf{z}_2) - f(\mathbf{z}_1) \quad \forall\, \mathbf{z}_1, \mathbf{z}_2 \in \mathbb{K}.$$

2. Consistency.
$$\mathrm{D}_{\mathbf{z}} f(\mathbf{z}_1, \mathbf{z}_2) = \partial_{\mathbf{z}} f(\bar{\mathbf{z}}) + \mathcal{O}(\|\mathbf{z}_2 - \mathbf{z}_1\|),$$
where $\bar{\mathbf{z}} := \frac{1}{2}(\mathbf{z}_1 + \mathbf{z}_2)$.

There is not necessarily a single unique function which satisfies this definition. However, the construction adopted here is similar to that of [24], [25]. The discrete derivative is evaluated as
$$\mathrm{D}_{\mathbf{z}} f(\mathbf{z}_1, \mathbf{z}_2) := \overline{\partial_{\mathbf{z}} f} + \left[\frac{f(\mathbf{z}_2) - f(\mathbf{z}_1) - \overline{\partial_{\mathbf{z}} f}}{\|\mathbf{z}_2 - \mathbf{z}_1\|^2}\right](\mathbf{z}_2 - \mathbf{z}_1), \tag{75}$$
where $\overline{\partial_{\mathbf{z}} f}$ satisfies
$$\overline{\partial_{\mathbf{z}} f} = \partial_{\mathbf{z}} f\,(\bar{\mathbf{z}}) + \mathcal{O}(\|\mathbf{z}_2 - \mathbf{z}_1\|). \tag{76}$$
Two possible options are

1. Midpoint approximation:
$$\overline{\partial_{\mathbf{z}} f} := \partial_{\mathbf{z}} f(\bar{\mathbf{z}}). \tag{77}$$
This is the form adopted in [24], [25].

2. Trapezoidal approximation:
$$\overline{\partial_{\mathbf{z}} f} := \frac{1}{2}\left[\partial_{\mathbf{z}} f(\mathbf{z}_1) + \partial_{\mathbf{z}} f(\mathbf{z}_2)\right]. \tag{78}$$

Either option satisfies (76) and ensures that $\mathrm{D}_{\mathbf{z}} f(\mathbf{z}_1, \mathbf{z}_2)$ has a well defined limit as $\|\mathbf{z}_2 - \mathbf{z}_1\| \searrow 0$. If a positive term $\mathcal{D} > 0$ is added to (75) so that the discrete derivative has the modified form
$$\mathrm{D}_{\mathbf{z}} f(\mathbf{z}_1, \mathbf{z_2}) := \overline{\partial_{\mathbf{z}} f} + \left[\frac{f(\mathbf{z}_2) - f(\mathbf{z_1}) + \mathcal{D} - \overline{\partial_{\mathbf{z}} f}}{\|\mathbf{z}_2 - \mathbf{z}_1\|^2}\right](\mathbf{z}_2 - \mathbf{z}_1), \tag{79}$$
then
$$\mathrm{D}_{\mathbf{z}} f(\mathbf{z}_1, \mathbf{z_2}) \cdot (\mathbf{z}_2 - \mathbf{z}_1) = f(\mathbf{z}_2) - f(\mathbf{z}_1) + \mathcal{D} \geq f(\mathbf{z}_2) - f(\mathbf{z}_1) \quad \forall\, \mathbf{z}_1, \mathbf{z}_2 \in \mathbb{K} \tag{80}$$

3.3.1 Algorithmic stress

A symmetric *algorithmic stress* is defined as [35]

$$\boxed{\mathbf{S}^{dev}_{algo} := \bar{\mathbf{S}} + \left[\frac{2\left(\widetilde{W}(\mathbf{b}^e_{n+1},\xi_{n+1}) - \widetilde{W}(\mathbf{b}^e_n,\xi_n) + \Delta\mathcal{D}^{int}\right) - \bar{\mathbf{S}} : \Delta\mathbf{C}}{\|\Delta\mathbf{C}\|^2}\right]\Delta\mathbf{C}}, \tag{81}$$

where

$$\boxed{\bar{\mathbf{S}} := \frac{1}{2}\left[\boldsymbol{\varphi}^*_n(\operatorname{dev}\boldsymbol{\tau}_n) + \boldsymbol{\varphi}^*_{n+1}(\operatorname{dev}\boldsymbol{\tau}_{n+1})\right]}. \tag{82}$$

This definition makes use of the notion of a discrete derivative of $\widetilde{W}$ to define $\mathbf{S}^{dev}_{algo}$. Furthermore, the utility of the discrete derivative is seen in the following easily verified inequality

$$\frac{1}{2}\mathbf{S}^{dev}_{algo} : \Delta\mathbf{C} = \Delta\widetilde{W} + \Delta\mathcal{D}^{int} \geq \Delta\widetilde{W}. \tag{83}$$

Thus $\mathbf{S}^{dev}_{algo}$ satisfies by construction a time-discrete form of the dissipation inequality (24) and shall be used, along with discrete derivatives of $J(\mathbf{C})$ and $U(\Theta)$, to ensure energy consistency of the dynamic MPM time stepping algorithm for (13).

Remarks 3.2.

1. The addition of a dissipation term $\mathcal{D} > 0$ to the discrete derivative has been used previously in [4], [5] to add controllable high frequency dissipation to dynamic hyperelastic simulations.

2. In a seminal work, Meng & Laursen [35] consider a very similar formulation for dynamic finite deformation plasticity in a Lagrangian finite element setting. However, in that paper the authors make use of a midpoint integrator [49] for the plastic evolution equations. Consequently, the definition of $\bar{\mathbf{S}}$ takes the form

   $$\bar{\mathbf{S}} := \boldsymbol{\varphi}^*_{n+1/2}(\operatorname{dev}\boldsymbol{\tau}_{n+1/2}),$$

   which in the purely elastic case collapses to

   $$\bar{\mathbf{S}} = 2\partial_{\mathbf{C}}\widehat{W}\left(\mathbf{F}^T_{n+1/2}\mathbf{F}_{n+1/2}\right).$$

   Unfortunately, this form for $\bar{\mathbf{S}}$ may not have a well defined limit as $\|\Delta\mathbf{C}\| \searrow 0$ (see [30]). To avoid this possible problem, and for ease of implementation, a backward Euler integrator along with equation (82) is chosen for this work.

3. The general developments presented here are not restricted to isotropic multiplicative plasticity. The same algorithmic constructions can be applied to any hyperelastic-based, thermodynamically consistent material model. This includes, but is not limited to, additive Green-Naghdi plasticity [35], [42], finite strain viscoelasticity [45], anisotropic single crystal plasticity [38], [56] and continuum damage modeling [21], [48].

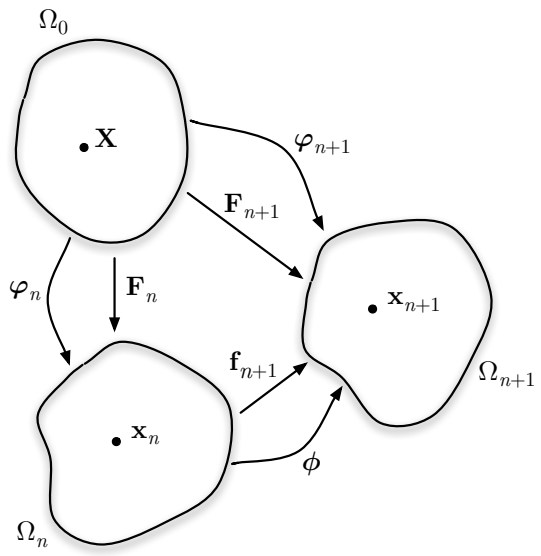

Figure 1: Diagram indicating the notation used to relate the reference configuration of the body with its configuration at times t_n and t_{n+1}. By this construction, $\boldsymbol{\varphi}_{n+1} = \boldsymbol{\phi} \circ \boldsymbol{\varphi}_n$ and $\mathbf{F}_{n+1} = \mathbf{f}_{n+1}\mathbf{F}_n$. Assuming the same fixed Cartesian coordinate system for all three configurations, $\boldsymbol{\phi} = \mathbf{id} + \Delta\boldsymbol{\varphi}$, where $\Delta\boldsymbol{\varphi} = (\boldsymbol{\varphi}_{n+1} - \boldsymbol{\varphi}_n) \circ \boldsymbol{\varphi}_n^{-1}$.

3.4 Discrete equations of motion

Denote by N^A the shape function of node A of the mesh. Let $\mathcal{W}^h \subset \mathcal{W}$ denote a typical finite dimensional finite element subspace of $\mathcal{W}$, with corresponding solution space $\mathcal{S}^h \subset \mathcal{S}$. Then, for example, any $\delta\boldsymbol{\varphi}^h \in \mathcal{W}^h$ takes the form

$$\delta\boldsymbol{\varphi}^h(\mathbf{x}) = \sum_{A=1}^{N_{nodes}} N^A(\mathbf{x})\delta\boldsymbol{\varphi}_A. \tag{84}$$

All integrals are evaluated by treating the material points as quadrature points. For example, the second term in (13a) can be approximated as

$$\left.\begin{aligned} \mathbf{B}^h(\mathbf{x}) := \mathrm{GRAD}_{\mathbf{X}}[\delta\boldsymbol{\varphi}^h(\mathbf{x})] = \sum_{A=1}^{N_{nodes}} \delta\boldsymbol{\varphi}_A \otimes \left(\mathbf{F}_n^T(\mathbf{x})\ \mathrm{grad}_n[N^A(\mathbf{x})]\right) \\ \langle \mathrm{GRAD}_{\mathbf{X}}[\delta\boldsymbol{\varphi}], \mathbf{F}_{n+\alpha}\mathbf{S}\rangle_{\Omega_0} \approx \sum_{pt=1}^{N_{pt}} \left(\mathbf{B}^h(\mathbf{x}_n^{pt}) : \mathbf{F}_{n+\alpha}^{pt}\mathbf{S}^{pt}\right) \Omega_0^{pt} \end{aligned}\right\}, \tag{85}$$

where $\mathbf{x}_n^{pt} = \boldsymbol{\varphi}_n^{pt}$ is the material-point position at time step n and $\Omega_0^{pt} > 0$ is the material volume associated with the material point pt. The transformation $\mathrm{GRAD}_{\mathbf{X}}[\cdot] = \mathbf{F}_n^T\,\mathrm{grad}_n[\cdot]$ is also used, where grad_n indicates the gradient with respect to the configuration at time t_n. Figure 1 schematically shows the notation used to relate the reference configuration of the deforming body with its configuration at times t_n and t_{n+1}.

The mass $m^{pt} = \rho_0(\mathbf{x}^{pt})\Omega_0^{pt} > 0$ is constant for each material point. The material-point momentum is then $\boldsymbol{\pi}^{pt} := m^{pt}\mathbf{v}^{pt}$. Using the material-point masses, the *consistent* mass matrix $\mathbf{M}$ is defined with nodal components

$$M^{AB} := \sum_{pt=1}^{N_{pt}} m^{pt} N^A(\mathbf{x}^{pt}) N^B(\mathbf{x}^{pt}) \approx \int_{\Omega_0} \rho_0 N^A N^B \, \mathrm{d}\Omega_0. \tag{86}$$

Remarks 3.3. Many MPM implementations use a lumped mass matrix [26],[57],[58], [59],[60], [63]. However, in an effort to ensure that global conservation properties are satisfied [14], [30], only the consistent mass matrix is considered in this work.

Given the material-point data $\{\boldsymbol{\varphi}_n^{pt}, \mathbf{v}_n^{pt}, \mathbf{F}_n^{pt}, \Theta_n^{pt}, \mathbf{G}_n^p, \xi_n\}$ at time t_n, the goal is to determine the material-point data $\{\boldsymbol{\varphi}_{n+1}^{pt}, \mathbf{v}_{n+1}^{pt}, \mathbf{F}_{n+1}^{pt}, \Theta_{n+1}^{pt}, \mathbf{G}_{n+1}^p, \xi_{n+1}\}$ at time $\mathrm{t}_{n+1} := \mathrm{t}_n + \Delta\mathrm{t}$. Assuming a background finite element mesh exists, the MPM algorithm is as follows:

Algorithm MPM. The algorithm consists of four primary steps:

1. *Material-Point-to-Grid Projection.* Compute the consistent mass matrix $\mathbf{M}_n$ using (86). Compute the grid velocities $\mathbf{v}_n^h$ such that

$$\sum_{B=1}^{N_{nodes}} M_n^{AB} \mathbf{v}_{B,n} = \sum_{pt=1}^{N_{pt}} N^A(\mathbf{x}_n^{pt}) \boldsymbol{\pi}_n^{pt} \;\; \forall A \in \{1, 2, \ldots, N_{nodes}\}. \tag{87}$$

2. *Lagrangian Mesh Dynamics.* Solve the nonlinear algebraic equations

$$\frac{1}{\Delta\mathrm{t}} \sum_{B=1}^{N_{nodes}} M_n^{AB} \left(\mathbf{v}_{B,n+1} - \mathbf{v}_{B,n}\right) + \left(\mathbf{F}^{int}\right)_{n+1/2}^A - \left(\mathbf{F}^{ext}\right)_{n+1/2}^A = \mathbf{0}, \tag{88a}$$

$$\frac{1}{\Delta\mathrm{t}} \Delta\boldsymbol{\varphi}_A = \mathbf{v}_{A,n+1/2}, \tag{88b}$$

$$\sum_{pt=1}^{N_{pt}} \delta\theta^h(\boldsymbol{\varphi}_n^{pt}) \cdot \left[p^h(\boldsymbol{\varphi}_n^{pt}) - \mathrm{D}_\Theta U(\Theta_n^{pt}, \Theta_{n+1}^{pt})\right] \; \Omega_0^{pt} = 0, \tag{88c}$$

$$\sum_{pt=1}^{N_{pt}} \delta p^h(\boldsymbol{\varphi}_n^{pt}) \cdot \left[\theta^h(\boldsymbol{\varphi}_n^{pt}) - \Delta J^{pt}\right] \; \Omega_0^{pt} = 0, \tag{88d}$$

$$\Theta_{n+1}^{pt} = \Theta_n^{pt} + \theta^h(\boldsymbol{\varphi}_n^{pt}), \tag{88e}$$

for $A \in \{1, 2, \ldots, N_{nodes}\}$, where $(\mathbf{F}^{int})_{n+1/2}^A$ and $(\mathbf{F}^{ext})_{n+1/2}^A$ are the internal and external forces, respectively, associated with node A at time $\mathrm{t}_{n+1/2}$. These forces are defined as

$$\left.\begin{aligned} \left(\mathbf{F}^{int}\right)_{n+1/2}^A &:= \sum_{pt=1}^{N_{pt}} \left(\mathbf{F}_{n+1/2}^{pt} \mathbf{S}^h\right) \left(\mathbf{F}_n^{pt}\right)^T \mathrm{grad}_n[N^A(\mathbf{x}_n^{pt})] \, \Omega_0^{pt} \\ &\approx \int_{\Omega_0} \left(\mathbf{F}_{n+1/2} \mathbf{S}^h\right) \mathrm{GRAD}_{\mathbf{X}}[N^A] \, \mathrm{d}\Omega_0 \end{aligned}\right\}, \tag{89a}$$

$$\left.\begin{aligned}\big(\mathbf{F}^{ext}\big)^A_{n+1/2} &:= \sum_{pt=1}^{N_{pt}} m^{pt}\mathbf{b}_{n+1/2}N^A(\mathbf{x}^{pt}_n) + \bar{\mathbf{T}}^A_{n+1/2} \\ &\approx \int_{\Omega_0} N^A\rho_0\mathbf{b}_{n+1/2}\,\mathrm{d}\Omega_0 + \int_{\Gamma_{\boldsymbol{\sigma}}} N^A\bar{\mathbf{T}}_{n+1/2}\,\mathrm{d}\Gamma_0\end{aligned}\right\}, \tag{89b}$$

where

$$\mathbf{S}^h := \mathbf{S}^{dev}_{algo} \;+\; 2p^h(\boldsymbol{\varphi}^{pt}_n)\cdot \mathrm{D}_{\mathbf{C}}J(\mathbf{C}^{pt}_n, \mathbf{C}^{pt}_{n+1}), \tag{90}$$

and $\bar{\mathbf{T}}^A_{n+1/2}$ is an approximation to the nodal value of the surface traction, $\bar{\mathbf{T}}^A_{n+1/2} \approx \int_{\Gamma_{\boldsymbol{\sigma}}} N^A\bar{\mathbf{T}}_{n+1/2}\,\mathrm{d}\Gamma_0$. The mixed variational fields $\{p^h, \theta^h\}$ are *not particle based*. In an effort to avoid an overconstrained pressure field, which can lead to locking of a finite element approximation, $\{p^h, \theta^h\}$ and their corresponding variations are chosen to be *piecewise constant* on each background finite element [54]. Notice that

$$\sum_{pt=1}^{N_{pt}} \delta\theta^h(\boldsymbol{\varphi}^{pt}_n)\cdot\big[p^h(\boldsymbol{\varphi}^{pt}_n) - \mathrm{D}_\Theta U(\Theta^{pt}_n, \Theta^{pt}_{n+1})\big]\;\Omega^{pt}_0 \approx \langle\, \delta\theta, p - \mathrm{D}_\Theta U(\Theta_n, \Theta_{n+1})\,\rangle_{\Omega_0},$$

and

$$\sum_{pt=1}^{N_{pt}} \delta p^h(\boldsymbol{\varphi}^{pt}_n)\cdot\big[\theta^h(\boldsymbol{\varphi}^{pt}_n) - \Delta J^{pt}\big]\;\Omega^{pt}_0 \approx \langle \delta p, \theta - \Delta J\rangle_{\Omega_0}.$$

During this step, the deformation gradient for each material point is multiplicatively updated via

$$\left.\begin{aligned}\mathbf{f}^h_{n+1}(\mathbf{x}_n) &:= \mathbf{I} + \mathrm{grad}_n\big[\Delta\boldsymbol{\varphi}^h(\mathbf{x}_n)\big] \\ \mathbf{F}^{pt}_{n+1} &:= \mathbf{f}^h_{n+1}(\mathbf{x}^{pt}_n)\;\mathbf{F}^{pt}_n\end{aligned}\right\}. \tag{91}$$

The above equations of this step, all together, are the Galerkin spatial projection of the weak form (13) onto the finite element subspace, coupled with an incremental midpoint-based time stepping scheme.

3. *Material-Point Update*. Update the material-point positions and velocities via

$$\left.\begin{aligned}\boldsymbol{\varphi}^{pt}_{n+1} &= \;\boldsymbol{\varphi}^{pt}_n + \Delta\boldsymbol{\varphi}^h(\mathbf{x}^{pt}_n) \\ \mathbf{v}^{pt}_{n+1} &= \;\mathbf{v}^{pt}_n + \Delta\mathbf{v}^h(\mathbf{x}^{pt}_n)\end{aligned}\right\}. \tag{92}$$

4. *Regrid*. During step 2, the finite element mesh deforms. During step 4, the mesh may be moved, if desired. In particular, the mesh may be returned to the position it occupied at the beginning of step 2. This choice is typical of many MPM implementations. Alternatively, the mesh may be redefined to suit any requirements the user may have, including the enforcement of Dirichlet boundary conditions, or adaption to features of the solution.

(End Algorithm MPM) ♦

Remarks 3.4.

1. Equations (88c) - (88e) are solved at the element level and do not explicitly enter the global system of equations (88a) [54].

2. Equations (88d) - (88e) are not necessarily the only method for updating the element level mixed volume. Alternative formulations are discussed in Appendix A. Unfortunately, the energy conservation properties of the alternatives are unclear.

3. Unfortunately, the four-node constant pressure/volume quadrilateral (Q1/P0) finite element *does not satisfy the inf-sup(LBB) condition* [13]. The existence of well known pressure *checkerboard modes* [20], [40] precludes satisfaction of the LBB stability criterion. However, this ill-conditioning appears to be restricted to the pressure field and the velocity field is very often still convergent (Theorem 10.3.7 of [12] and [33]). A convergent pressure field can often be recovered by filtering or smoothing the oscillatory pressures [15], [28], [33], [46], [47]. Despite this shortcoming, the Q1/P0 quadrilateral remains popular in computational solid mechanics and is a relatively simple element formulation which avoids volumetric locking.

3.5 Conservation properties

Definition 3.2. The *total grid (mesh) linear momentum* $\mathbf{L}^h$ is defined as

$$\mathbf{L}^h := \sum_{A=1}^{N_{nodes}} \left(\sum_{B=1}^{N_{nodes}} M^{AB} \mathbf{v}_B \right) \tag{93}$$

Definition 3.3. The *total material-point linear momentum* $\mathbf{L}^{pt}$ is defined as

$$\mathbf{L}^{pt} := \sum_{pt=1}^{N_{pt}} \boldsymbol{\pi}^{pt}. \tag{94}$$

Definition 3.4. The *total grid (mesh) angular momentum* $\mathbf{J}^h$ is defined as

$$\mathbf{J}^h := \sum_{A=1}^{N_{nodes}} \left(\boldsymbol{\varphi}_A \times \sum_{B=1}^{N_{nodes}} M^{AB} \mathbf{v}_B \right). \tag{95}$$

Definition 3.5. The *total material-point angular momentum* $\mathbf{J}^{pt}$ is defined as

$$\mathbf{J}^{pt} := \sum_{pt=1}^{N_{pt}} \left(\boldsymbol{\varphi}^{pt} \times \boldsymbol{\pi}^{pt} \right) = \sum_{pt=1}^{N_{pt}} \left(\mathbf{x}^{pt} \times \boldsymbol{\pi}^{pt} \right). \tag{96}$$

Definition 3.6. The *total grid (mesh) kinetic energy* T^h is defined as

$$2\mathsf{T}^h := \sum_{A=1}^{N_{nodes}} \left(\mathbf{v}_A \cdot \sum_{B=1}^{N_{nodes}} M^{AB} \mathbf{v}_B \right). \tag{97}$$

Definition 3.7. The *total material-point kinetic energy* T^{pt} is defined as

$$2\mathsf{T}^{pt} := \sum_{pt=1}^{N_{pt}} \left(\boldsymbol{\pi}^{pt} \cdot \frac{1}{m^{pt}} \boldsymbol{\pi}^{pt} \right) = \sum_{pt=1}^{N_{pt}} \left(\boldsymbol{\pi}^{pt} \cdot \mathbf{v}^{pt} \right) = \sum_{pt=1}^{N_{pt}} m^{pt} \|\mathbf{v}^{pt}\|^2 \tag{98}$$

Definition 3.8. The *total material-point potential energy* V^{pt} is defined as

$$\mathsf{V}^{pt} := \sum_{pt=1}^{N_{pt}} \left[\widetilde{W}(\mathbf{b}^e, \xi) + U(\Theta^{pt}) \right] \Omega_0^{pt}. \tag{99}$$

Definition 3.9. The *total grid (mesh) energy* H^h is defined as

$$\mathsf{H}^h := \mathsf{T}^h + \mathsf{V}^{pt}. \tag{100}$$

Definition 3.10. The *total material-point energy* H^{pt} is defined as

$$\mathsf{H}^{pt} := \mathsf{T}^{pt} + \mathsf{V}^{pt}. \tag{101}$$

Remarks 3.5. There is no need to draw a distinction between total potential energy defined on the grid and total potential energy defined on the material points. They are in fact the same quantity. To compute the total grid potential energy one would use the material points as quadrature points for the integral, and the result would be exactly V^{pt}.

Linear and angular momentum conservation are fairly straightforward and the fact that these quantities are conserved has been shown previously in the references [24], [30], [53].

Proposition 3.1. Assume $(\mathbf{F}^{ext})^A_{n+1/2} = \mathbf{0}$. Then the mesh dynamics conserve exactly the total mesh linear momentum and total mesh angular momentum. Additionally, assume that the algorithmic stress satisfies the discrete dissipation inequality (83). Then the mesh dynamics dissipate the total mesh energy,

$$\mathsf{H}^h_{n+1} = \mathsf{H}^h_n - \sum_{pt=1}^{N_{pt}} \Delta\mathcal{D}^{int} \cdot \Omega_0^{pt} \leq \mathsf{H}^h_n \,, \tag{102}$$

so that $\Delta\mathsf{H}^h = \Delta\mathsf{T}^h + \Delta\mathsf{V}^h \leq 0$.

Proof.

1. *Linear Momentum is conserved.* See [24], [30].

2. *Angular Momentum is conserved.* This is a direct consequence of the symmetry of $\mathbf{S}^h$ [24], [30].

3. *Energy is dissipated.* The presentation follows closely that of Proposition 5 in [24]. First, since $\widetilde{\mathbf{M}}$ is symmetric, note that the change in kinetic energy can be written

$$\begin{aligned}
\Delta \mathsf{T}^h &= \mathsf{T}^h_{n+1} - \mathsf{T}^h_n \\
&= \frac{1}{2}\sum_{A,B=1}^{N_{nodes}} (\mathbf{v}_{A,n} + \mathbf{v}_{A,n+1}) \cdot \widetilde{M}^{AB}_n (\mathbf{v}_{B,n+1} - \mathbf{v}_{B,n}) \\
&= \sum_{A,B=1}^{N_{nodes}} \mathbf{v}_{A,n+1/2} \cdot \widetilde{M}^{AB}_n (\mathbf{v}_{B,n+1} - \mathbf{v}_{B,n}).
\end{aligned} \tag{103}$$

Use equations (88c) (88d) (88e) (83) (90):

$$\begin{aligned}
\Delta \mathsf{V}^{pt} &= \mathsf{V}^{pt}_{n+1} - \mathsf{V}^{pt}_n \\
&= \sum_{pt=1}^{N_{pt}} \left[\widetilde{W}(\mathbf{b}^e_{n+1}, \xi_{n+1}) + U(\Theta^{pt}_{n+1}) - \widetilde{W}(\mathbf{b}^e_n, \xi_n) - U(\Theta^{pt}_n) \right] \Omega^{pt}_0 \\
&= \sum_{pt=1}^{N_{pt}} \left[\frac{1}{2}(\mathbf{C}^{pt}_{n+1} - \mathbf{C}^{pt}_n) : \mathbf{S}^{dev}_{algo} + \mathrm{D}_\Theta U(\Theta^{pt}_n, \Theta^{pt}_n) \cdot \Delta\Theta^{pt} - \Delta\mathcal{D}^{int} \right] \Omega^{pt}_0 \\
&= \sum_{pt=1}^{N_{pt}} \left[\frac{1}{2}\left(\mathbf{C}^{pt}_{n+1} - \mathbf{C}^{pt}_n\right) : \mathbf{S}^{dev}_{algo} + p^h(\boldsymbol{\varphi}^{pt}_n) \cdot \theta^h(\boldsymbol{\varphi}^{pt}_n) - \Delta\mathcal{D}^{int} \right] \Omega^{pt}_0 \\
&= \sum_{pt=1}^{N_{pt}} \left[\frac{1}{2}\left(\mathbf{C}^{pt}_{n+1} - \mathbf{C}^{pt}_n\right) : \mathbf{S}^{dev}_{algo} + p^h(\boldsymbol{\varphi}^{pt}_n) \cdot \Delta J^{pt} - \Delta\mathcal{D}^{int} \right] \Omega^{pt}_0 \\
&= \sum_{pt=1}^{N_{pt}} \left[\frac{1}{2}\left(\mathbf{C}^{pt}_{n+1} - \mathbf{C}^{pt}_n\right) : \mathbf{S}^{dev}_{algo} \right] \Omega^{pt}_0 \\
&\qquad + \sum_{pt=1}^{N_{pt}} \left[\frac{1}{2}(\mathbf{C}^{pt}_{n+1} - \mathbf{C}^{pt}_n) : 2p^h(\boldsymbol{\varphi}^{pt}_n) \cdot \mathrm{D}_{\mathbf{C}} J(\mathbf{C}^{pt}_n, \mathbf{C}^{pt}_{n+1}) - \Delta\mathcal{D}^{int} \right] \Omega^{pt}_0 \\
&= \sum_{pt=1}^{N_{pt}} \left[\frac{1}{2}\left(\mathbf{C}^{pt}_{n+1} - \mathbf{C}^{pt}_n\right) : \mathbf{S}^h - \Delta\mathcal{D}^{int} \right] \Omega^{pt}_0 .
\end{aligned} \tag{104}$$

$$
\begin{aligned}
\Delta \mathrm{V}^{pt} &= \sum_{pt=1}^{N_{pt}} \left[\frac{1}{2} \left(\mathbf{C}_{n+1}^{pt} - \mathbf{C}_{n}^{pt} + \underbrace{(\mathbf{F}_{n}^{pt})^T \mathbf{F}_{n+1}^{pt} - (\mathbf{F}_{n+1}^{pt})^T \mathbf{F}_{n}^{pt}}_{\text{skew}} \right) : \mathbf{S}^h - \Delta \mathcal{D}^{int} \right] \Omega_0^{pt} \\
&= \sum_{pt=1}^{N_{pt}} \left[\frac{1}{2} \left(\mathbf{F}_{n}^{pt} + \mathbf{F}_{n+1}^{pt} \right)^T \left(\mathbf{F}_{n+1}^{pt} - \mathbf{F}_{n}^{pt} \right) : \mathbf{S}^h - \Delta \mathcal{D}^{int} \right] \Omega_0^{pt} \\
&= \sum_{pt=1}^{N_{pt}} \left[\left(\mathbf{F}_{n+1}^{pt} - \mathbf{F}_{n}^{pt} \right) : \mathbf{F}_{n+1/2}^{pt} \mathbf{S}^h - \Delta \mathcal{D}^{int} \right] \Omega_0^{pt} \\
&= \sum_{pt=1}^{N_{pt}} \left[\mathrm{grad}_n \left[\Delta \boldsymbol{\varphi}^h(\mathbf{x}_n^{pt}) \right] \mathbf{F}_{n}^{pt} : \mathbf{F}_{n+1/2}^{pt} \mathbf{S}^h - \Delta \mathcal{D}^{int} \right] \Omega_0^{pt} \\
&= \sum_{pt=1}^{N_{pt}} \sum_{A=1}^{N_{nodes}} \left(\left[\Delta \boldsymbol{\varphi}_A \otimes \mathrm{grad}_n [N^A(\mathbf{x}_n^{pt})] \right] \mathbf{F}_{n}^{pt} \right) : (\mathbf{F}_{n+1/2}^{pt} \mathbf{S}^h) \Omega_0^{pt} - \sum_{pt=1}^{N_{pt}} \Delta \mathcal{D}^{int} \Omega_0^{pt} \\
&= \sum_{A=1}^{N_{nodes}} \sum_{pt=1}^{N_{pt}} \Delta \boldsymbol{\varphi}_A \cdot \left(\mathbf{F}_{n+1/2}^{pt} \mathbf{S}^h \right) \underbrace{(\mathbf{F}_{n}^{pt})^T \mathrm{grad}_n [N^A(\mathbf{x}_n^{pt})]}_{\mathrm{GRAD}_{\mathbf{X}} \left[N^A(\mathbf{x}_n^{pt}) \right]} \Omega_0^{pt} - \sum_{pt=1}^{N_{pt}} \Delta \mathcal{D}^{int} \Omega_0^{pt} \\
&= \sum_{A=1}^{N_{nodes}} \mathbf{v}_{A,n+1/2} \Delta \mathrm{t} \cdot \sum_{pt=1}^{N_{pt}} \left(\mathbf{F}_{n+1/2}^{pt} \mathbf{S}^h \right) (\mathbf{F}_{n}^{pt})^T \mathrm{grad}_n [N^A(\mathbf{x}_n^{pt})] \Omega_0^{pt} - \sum_{pt=1}^{N_{pt}} \Delta \mathcal{D}^{int} \Omega_0^{pt} \\
&= \Delta \mathrm{t} \sum_{A=1}^{N_{nodes}} \mathbf{v}_{A,n+1/2} \cdot \left(\mathbf{F}^{int} \right)_{n+1/2}^{A} - \sum_{pt=1}^{N_{pt}} \Delta \mathcal{D}^{int} \Omega_0^{pt}. \qquad (105)
\end{aligned}
$$

Finally, consideration of equation (88a) yields

$$
\begin{aligned}
0 &= \sum_{A=1}^{N_{Nodes}} \mathbf{v}_{A,n+1/2} \cdot \left[\frac{1}{\Delta \mathrm{t}} \sum_{B=1}^{N_{Nodes}} \widetilde{M}_n^{AB} \left(\mathbf{v}_{B,n+1} - \mathbf{v}_{B,n} \right) + \left(\mathbf{F}^{int} \right)_{n+1/2}^{A} \right] \\
&= \frac{1}{\Delta \mathrm{t}} (\mathsf{T}_{n+1}^h - \mathsf{T}_n^h) + \frac{1}{\Delta \mathrm{t}} (\mathsf{V}_{n+1}^{pt} - \mathsf{V}_n^{pt}) + \frac{1}{\Delta \mathrm{t}} \sum_{pt=1}^{N_{pt}} \Delta \mathcal{D}^{int} \Omega_0^{pt} \\
&= \frac{1}{\Delta \mathrm{t}} (\mathsf{H}_{n+1}^h - \mathsf{H}_n^h) + \frac{1}{\Delta \mathrm{t}} \sum_{pt=1}^{N_{pt}} \Delta \mathcal{D}^{int} \Omega_0^{pt} \qquad (106)
\end{aligned}
$$

Since $\Delta \mathrm{t} > 0$, $\mathsf{H}_{n+1}^h \leq \mathsf{H}_n^h$, which is the desired result.

□

Corollary 3.2. Algorithm MPM conserves exactly the total material-point linear momentum and the total material-point angular momentum. The total material-point energy is unconditionally dissipated,

$$
\boxed{\mathrm{H}_{n+1}^{pt} = \mathrm{H}_n^{pt} - \sum_{pt=1}^{N_{pt}} \Delta \mathcal{D}^{int} \cdot \Omega_0^{pt} \leq \mathrm{H}_n^{pt}}. \qquad (107)
$$

Proof. See [30], where it is shown that MPM with a consistent mass matrix inherits the conservation properties of the grid solution. □

4 Numerical simulations

The goal of this section is to present some relatively simple numerical simulations which demonstrate the conservation properties of Algorithm MPM. All numerical simulations in this work use a nonlinear quasi-Newton root finding algorithm coupled with a matrix-free iterative GMRES linear equation solving algorithm. These are provided by the computational library PETSc [7], [8], [9].

4.1 Impact of a Taylor bar

The classical Taylor bar problem [61], [64] is considered. This is a commonly simulated problem and is often used as a benchmark for transient dynamic computer codes [19], [23], [32]. A copper bar of radius 3.2mm and length 32.4mm impacts a rigid, frictionless wall with an initial longitudinal velocity of 0.227mm/μs. The material is modeled as elastoplastic with an elastic bulk modulus $K = 130.0$GPa and an elastic shear modulus $G = 43.3$GPa. The tension yield (flow) stress is $\sigma_Y = 0.4$GPa and linear hardening is assumed with $H = 0.1$GPa and $\eta = 0.0$Pa·s. The material has a density of $\rho_0 = 8.93\text{g/cm}^3$.

The bar moves within the rectangular domain $[0.0, 7.2] \times [0.0, 32.4]$, meshed by 9×50 elements. A constant time step of $\Delta t = 1.0\mu$s is used for the axisymmetric simulation. Eighty (80) time steps are performed. The time histories of radial and axial displacement are shown in Figure 2. The time history of energy is shown in Figure 3. Most numerical simulations of this problem are run for only $80\mu s$, at which time it has been observed that all the initial kinetic energy has been either dissipated or converted to potential energy. The results of this MPM simulation verify that observation. The sequence of deformed particle configurations, colored by contour values of equivalent plastic strain, are shown in Figure 4. All the results are consistent with those in [19], [23], [32], [35], [49].

4.2 Colliding cylinders

The second example simulates the collision of two identical cylinders in plane strain. Each cylinder has an initial radius of 1.0. The cylinders are initially located at {-1.05,0.0} and {1.05,0.0}, respectively. The left cylinder is given an initial velocity of {1.0,-0.1}. The right cylinder is initially at rest. The material parameters are $K = 133.3$, $G = 43.3$, $\sigma_Y = 10.0$, $H = 0.01$ and $\eta = 0.0$. The material has a density of $\rho_0 = 8.824$. This same problem is simulated using energy consistent plasticity and contact algorithms in [36].

The cylinders move within the rectangular domain $[-2.20, 2.728] \times [-1.44, 1.20]$, meshed by 28×22 elements. A constant time step of $\Delta t = 0.015$ is used for the simulation. One-hundred twenty (120) time steps are performed. Figure 5 shows the evolution of energy for the MPM simulation and Figure 6 shows the sequence of the deformed particle configurations, colored by contours of equivalent plastic strain. The results are in good agreement with [36].

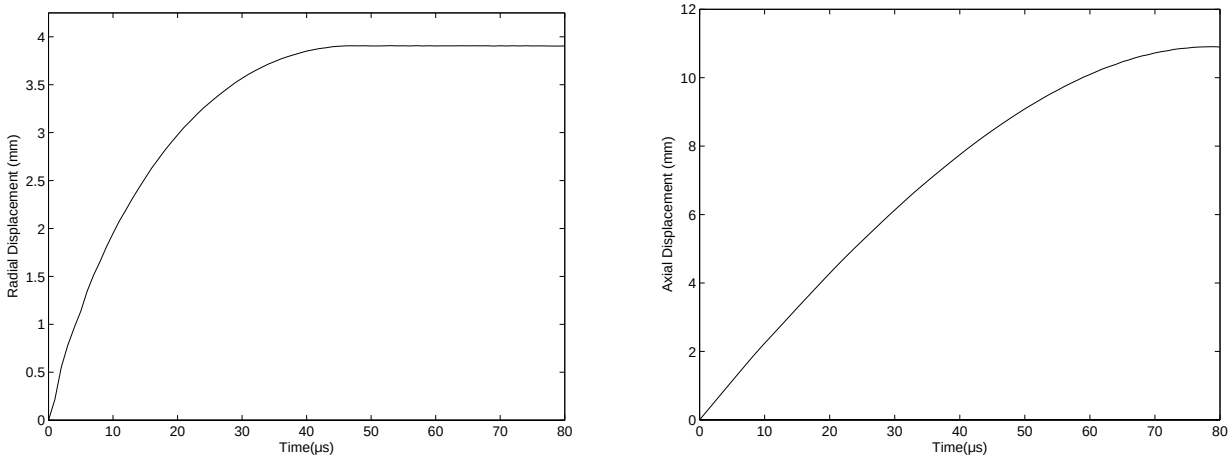

(a) Maximum radial displacement

(b) Maximum axial displacement

Figure 2: Impact of Taylor bar. Displacement history.

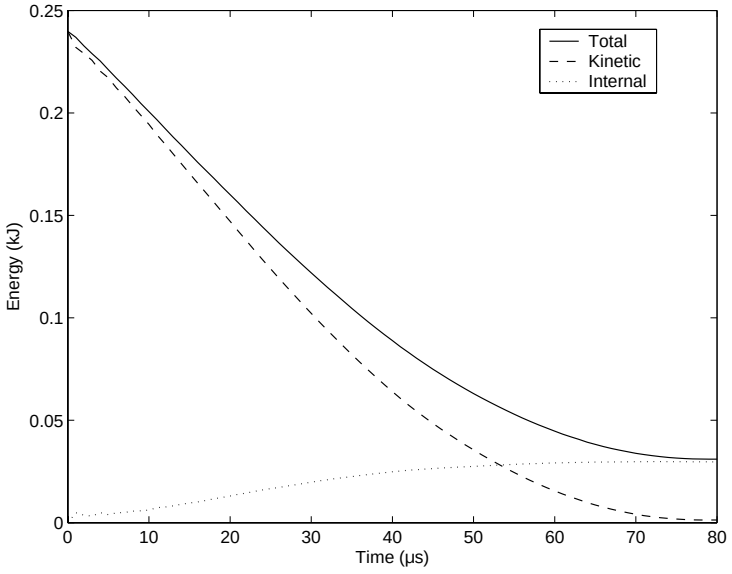

Figure 3: Impact of Taylor bar. Energy evolution.

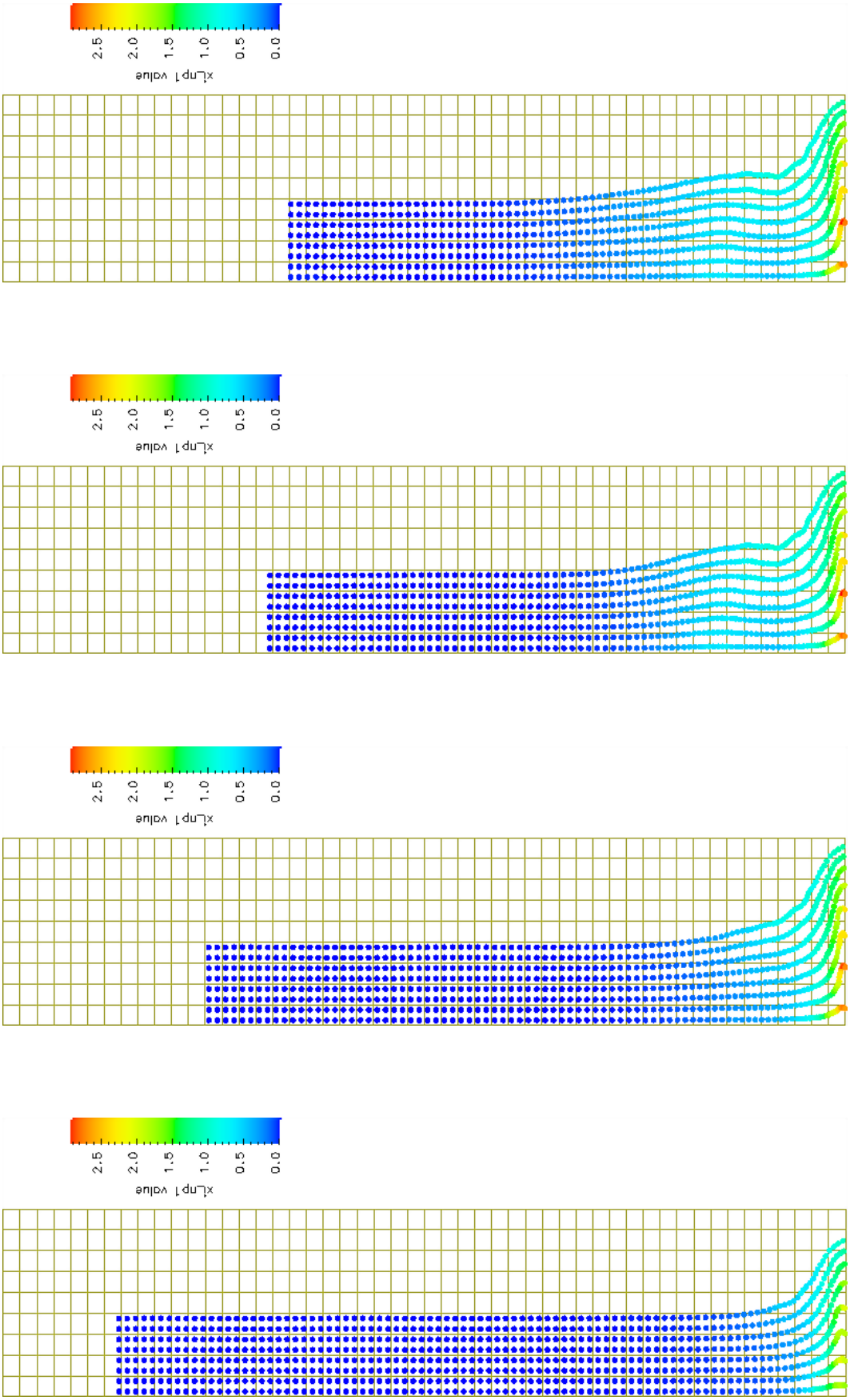

(a) Time t = $20\mu s$ (b) Time t = $40\mu s$ (c) Time t = $60\mu s$ (d) Time t = $80\mu s$

Figure 4: Impact of Taylor bar. Sequence of deformed particle configurations. Contours of equivalent plastic strain.

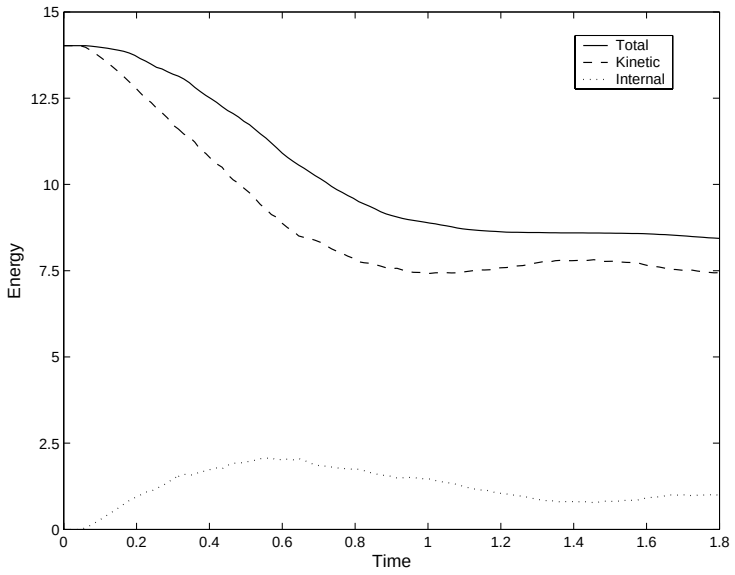

Figure 5: Colliding cylinders. Energy evolution.

There is no need to plot the time histories of linear or angular momentum for this example, as both are exactly conserved.

5 Closure

Energy consistency is examined for the MPM algorithm combined with a momentum conserving and energy dissipative finite element method for the grid dynamics. When a consistent mass matrix is used the MPM algorithm inherits the conservation properties of the grid solution. In particular, the implicit time integration scheme used for the grid dynamics is designed to reflect the continuum second law of thermodynamics, and conservation of linear and angular momenta. The conserving scheme applies to general hyperelastic-plastic material models and is applied to a multiplicative model of plasticity in the numerical examples. The numerical simulations confirm the theoretical behavior.

There are some logical extensions of this work. One might consider energy consistent algorithms for materials exhibiting localized dissipative mechanisms [2], [3]. A promising area is the simulation of Newtonian fluid dynamics, possibly with fluid-structure interaction. The MPM algorithm is more suited to flow calculations than Lagrangian finite element methods. It is also is of interest to examine frictional contact within MPM in the context of energy and momentum conserving methods. The frictional contact algorithms developed for MPM [10], [18] need modification to ensure that energy is consistently dissipated.

Acknowledgment: This material is based upon work supported by the National Science Foundation under Grant No. DMS-0222253. Any opinions, findings, and conclusions or recommendations expressed in this material are those of the author(s) and do not necessarily reflect the views of the National Science Foundation.

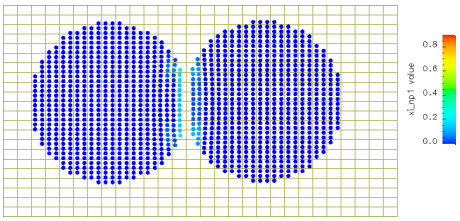

(a) Time t = 0.18

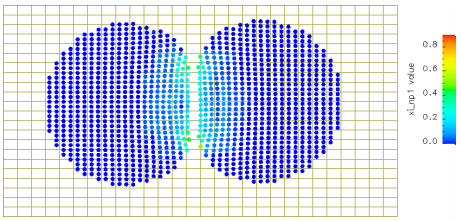

(b) Time t = 0.36

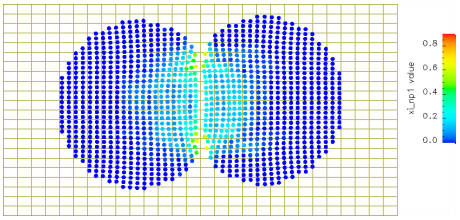

(c) Time t = 0.54

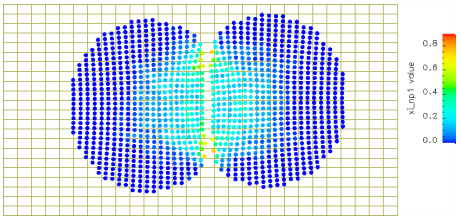

(d) Time t = 0.72

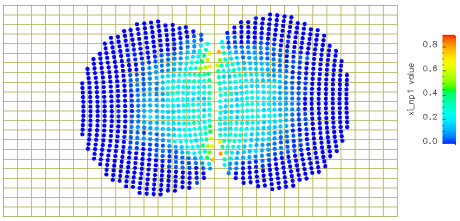

(e) Time t = 0.90

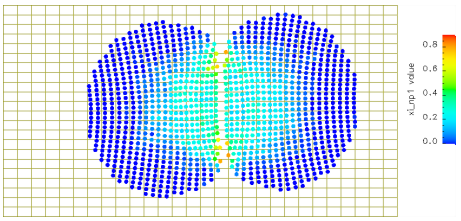

(f) Time t = 1.08

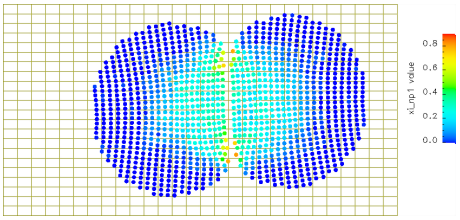

(g) Time t = 1.26

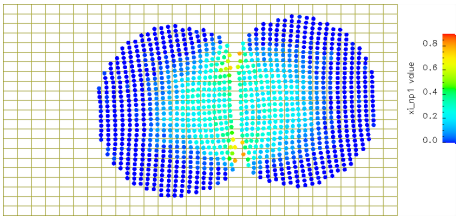

(h) Time t = 1.44

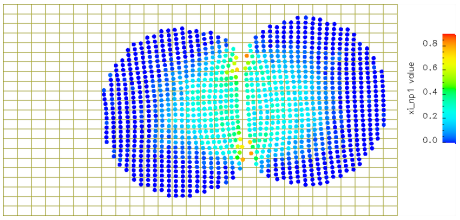

(i) Time t = 1.62

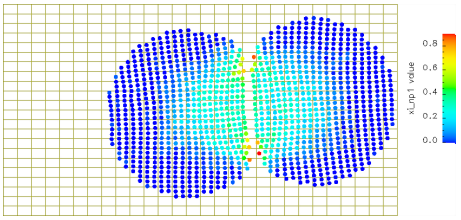

(j) Time t = 1.80

Figure 6: Colliding cylinders. Sequence of deformed particle configurations. Contours of equivalent plastic strain.

References

[1] Stuart S. Antman. *Nonlinear Problems of Elasticity*, volume 107 of *Applied Mathematical Sciences*. Springer-Verlag, New York, 1995.

[2] F. Armero. Large-scale modeling of localized dissipative mechanisms in a local continuum: applications to the numerical simulation of strain localization in rate-dependent inelastic solids. *Mechanics of Cohesive-Frictional Materials*, **4**(2):101–131, March 1999.

[3] F. Armero and K. Garikipati. An analysis of strong discontinuities in multiplicative finite strain plasticity and their relation with the numerical simulation of strain localization in solids. *International Journal of Solids and Structures*, **33**(20-22):2863–2885, August 1996.

[4] F. Armero and I. Romero. On the formulation of high-frequency dissipative time-stepping algorithms for nonlinear dynamics, part I: Low-order methods for two model problems and nonlinear elastodynamics. *Computer Methods in Applied Mechanics and Engineering*, **190**:2603–2649, 2001.

[5] F. Armero and I. Romero. On the formulation of high-frequency dissipative time-stepping algorithms for nonlinear dynamics, part II: Second-order methods. *Computer Methods in Applied Mechanics and Engineering*, **190**:6783–6824, 2001.

[6] Robert J. Asaro. Micromechanics of crystals and polycrystals. In John W. Hutchinson and Theodore Y. Wu, editors, *Advances in Applied Mechanics*, volume 23, pages 1–115. Academic Press, New York, 1983.

[7] Satish Balay, Kris Buschelman, Victor Eijkhout, William D. Gropp, Dinesh Kaushik, Matthew G. Knepley, Lois Curfman McInnes, Barry F. Smith, and Hong Zhang. PETSc users manual. Technical Report ANL-95/11 - Revision 2.1.5, Argonne National Laboratory, 2004.

[8] Satish Balay, Kris Buschelman, William D. Gropp, Dinesh Kaushik, Matthew G. Knepley, Lois Curfman McInnes, Barry F. Smith, and Hong Zhang. PETSc Web page, 2001. http://www.mcs.anl.gov/petsc.

[9] Satish Balay, Victor Eijkhout, William D. Gropp, Lois Curfman McInnes, and Barry F. Smith. Efficient management of parallelism in object oriented numerical software libraries. In E. Arge, A. M. Bruaset, and H. P. Langtangen, editors, *Modern Software Tools in Scientific Computing*, pages 163–202. Birkhäuser Press, 1997.

[10] S. Bardenhagen, J. Brackbill, and D. Sulsky. The material-point method for granular materials. *Computer Methods in Applied Mechanics and Engineering*, **187**:529–541, 2000.

[11] Ted Belytschko, Wing Kam Liu, and Brain Moran. *Nonlinear Finite Elements for Continua and Structures*. John Wiley and Sons, New York, 2000.

[12] Susanne C. Brenner and L. Ridgway Scott. *The Mathematical Theory of Finite Element Methods*, volume 15 of *Texts in Applied Mathematics*. Springer-Verlag, New York, 1994.

[13] Franco Brezzi and Michel Fortin. *Mixed and Hybrid Finite Element Methods*, volume 15 of *Springer Series in Computational Mathematics*. Springer-Verlag, New York, 1991.

[14] D. Burgess, D. Sulsky, and J. U. Brackbill. Mass matrix formulation of the FLIP particle-in-cell method. *Journal of Computational Physics*, **103**(1):1–15, 1992.

[15] Graham F. Carey and J. Tinsley Oden. *Finite Elements*, volume II: A second course. Prentice-Hall, Inc., Englewood Cliffs, NJ, 1983.

[16] Philippe G. Ciarlet. *Mathematical Elasticity, Volume I: Three-Dimensional Elasticity*, volume 20 of *Studies in Mathematics and its Applications*. North-Holland, New York, 1988.

[17] A. Cuitino and M. Ortiz. A material-independent method for extending stress update algorithms from small-strain plasticity to finite plasticity with multiplicative kinematics. *Enginering Computations*, **9**:437–451, 1992.

[18] S. J. Cummins and J. U. Brackbill. An implicit particle-in-cell method for granular materials. *Journal of Computational Physics*, **180**:506–548, 2002.

[19] Bruce E. Engelmann and John O. Hallquist. *Nike2D User Manual*. Lawrence Livermore National Laboratory, Livermore, CA, April 1991.

[20] Alexandre Ern and Jean-Luc Guermond. *Theory and Practice of Finite Elements*, volume 159 of *Applied Mathematical Sciences*. Springer-Verlag, New York, 2004.

[21] Lu Feng, Ke shi Zhang, Guang Zhang, and Hai dong Yu. Anisotropic damage model under continuum slip crystal plasticity theory for single crystals. *International Journal of Solids and Structures*, **39**(20):5279–5293, Ocotober 2002.

[22] Michel Fortin and Roland Glowinski. *Augmented Lagrangian Methods: Applications to the Numerical Solution of Boundary-Value Problems*, volume 15 of *Studies in Mathematics and its Applications*. North Holland, New York, 1983.

[23] M. S. Gadala. Recent trends in ALE formulation and its applications in solid mechanics. *Computer Methods in Applied Mechanics and Engineering*, **193**(39-41):4247–4275, October 2004.

[24] O. Gonzalez. Exact energy-momentum conserving algorithms for general models in nonlinear elasticity. *Computer Methods in Applied Mechanics and Engineering*, **190**:1763–1783, 2000.

[25] Oscar Gonzalez. *Design and Analysis of Conserving Integrators for Nonlinear Hamiltonian Systems with Symmetry*. PhD thesis, Department of Mechanical Engineering, Stanford University, Stanford, CA, 1996.

[26] J. E. Guilkey and J. A. Weiss. Implicit time integration for the material point method: Quantitative and algorithmic comparisons with the finite element method. *International Journal for Numerical Methods in Engineering*, **57**(9):1323–1338, July 2003.

[27] Morton E. Gurtin. *An Introduction to Continuum Mechanics*. Academic Press, New York, 1981.

[28] Thomas J. R. Hughes, Wing Kam Liu, and Alec Brooks. Finite element analysis of incompressible viscous flows by the penalty function formulation. *Journal of Computational Physics*, **30**(1):1–60, January 1979.

[29] E. H. Lee. Elastic-plastic deformations at finite strains. *ASME Journal of Applied Mechanics*, **36**:1–6, 1969.

[30] E. Love and D. L. Sulsky. An unconditionally stable, energy-momentum consistent implementation of the material-point method. Technical Report HPC@UNM2004-002, The Center for High Performance Computing, University of New Mexico, Albuquerque,NM, October 2004. (http://www.hpc.unm.edu).

[31] Jacob Lubliner. *Plasticity Theory*. Macmillan Publishing Company, New York, 1990.

[32] Bradley N. Maker, Robert N. Ferencz, and John O. Hallquist. *Nike3D User Manual*. Lawrence Livermore National Laboratory, Livermore, CA, April 1995.

[33] David S. Malkus and Elwood T. Olsen. Obtaining error estimates for optimally constrained incompressible finite elements. *Computer Methods in Applied Mechanics and Engineering*, **45**(1-3):331–353, September 1984.

[34] Jerrold E. Marsden and Thomas J. R. Hughes. *Mathematical Foundations of Elasticity*. Dover Publications, New York, 1994.

[35] X. N. Meng and T. A. Laursen. Energy consistent algorithms for dynamic finite deformation plasticity. *Computer Methods in Applied Mechanics and Engineering*, **191**(15-16):1639–1675, February 2002.

[36] X. N. Meng and T. A. Laursen. On energy consistency of large deformation plasticity models, with application to the design of unconditionally stable time integrators. *Finite Elements in Analysis and Design*, **38**:949–963, 2002.

[37] G. Meschke and W. N. Liu. A re-formulation of the exponential algorithm for finite strain plasticity in terms of Cauchy stresses. *Computer Methods in Applied Mechanics and Engineering*, **173**(1-2):167–187, April 1999.

[38] C. Miehe. Exponential map algorithm for stress updates in anisotropic multiplicative elastoplasticity for single crystals. *International Journal for Numerical Methods in Engineering*, **39**(19):3367–3390, October 1996.

[39] L. Moresi, F. Dufour, and H. B. Muhlhaus. A Lagrangian integration point finite element method for large deformation modeling of viscoelastic geomaterials. *Journal of Computational Physics*, **184**(2):476–497, January 2003.

[40] J. Tinsley Oden, Noboru Kikuchi, and Young Joon Song. Penalty-finite element methods for the analysis of Stokesian flows. *Computer Methods in Applied Mechanics and Engineering*, **31**(3):297–329, August 1982.

[41] R. W. Ogden. *Non-Linear Elastic Deformations*. Dover Publications, New York, 1997.

[42] Panayiotis Papadopoulos and Jia Lu. A general framework for the numerical solution of problems in finite elasto-plasticity. *Computer Methods in Applied Mechanics and Engineering*, **159**(1-2):1–18, July 1998.

[43] William H. Press, Brian P. Flannery, and Saul A. Teukolsky. *Numerical Recipes in C: The Art of Scientific Computing*. Cambridge University Press, New York, 2nd edition, 1995.

[44] S. Reese and P. Wriggers. A material model for rubber-like polymers exhibiting plastic deformation: computational aspects and a comparison with experimental results. *Computer Methods in Applied Mechanics and Engineering*, **148**(3-4):279–298, September 1997.

[45] Stefanie Reese and Sanjay Govindjee. A theory of finite viscoelasticity and numerical aspects. *International Journal of Solids and Structures*, **35**(26-27):3455–3482, September 1998.

[46] R. L. Sani, P. M. Gresho, R. L. Lee, and D. F. Griffiths. The cause and cure of the spurious pressures generated by certan FEM solutions of the incompressible Navier-Stokes equations, I. *International Journal for Numerical Methods in Fluids*, **1**(1):17–43, 1981.

[47] R. L. Sani, P. M. Gresho, R. L. Lee, D. F. Griffiths, and M. Engelman. The cause and cure of the spurious pressures generated by certan FEM solutions of the incompressible Navier-Stokes equations, II. *International Journal for Numerical Methods in Fluids*, **1**(2):171–204, 1981.

[48] J. C. Simo. On a fully three-dimensional finite-strain viscoelastic damage model: formulation and computational aspects. *Computer Methods in Applied Mechanics and Engineering*, **60**:153–173, 1987.

[49] J. C. Simo. Algorithms for static and dynamic multiplicative plasticity that preserve the classical return mapping schemes of the infinitesimal theory. *Computer Methods in Applied Mechanics and Engineering*, **99**(1):61–112, August 1992.

[50] J. C. Simo. Numerical analysis and simulation of plasticity. In P.G. Ciarlet and J. L. Lions, editors, *Handbook Of Numerical Analysis*, volume VI, pages 183–499. Elsevier, New York, 1998.

[51] J. C. Simo and T. J. R. Hughes. *Computational Inelasticity*, volume 7 of *Interdisciplinary Applied Mathematics*. Springer-Verlag, New York, August 1998.

[52] J. C. Simo and C. Miehe. Associative coupled thermoplasticity at finite strains: Formulation, numerical analysis and implementation. *Computer Methods in Applied Mechanics and Engineering*, **98**:41–104, 1992.

[53] J. C. Simo and N. Tarnow. The discrete energy-momentum method. Conserving algorithms for nonlinear elastodynamics. *Zeitschrift fur Angewandte Mathematik und Physik(ZAMP)*, **43**(5):757–792, September 1992.

[54] J. C. Simo and R. L. Taylor. Quasi-incompressible finite elasticity in principal stretches. Continuum basis and numerical algorithms. *Computer Methods in Applied Mechanics and Engineering*, **85**:273–310, 1991.

[55] J. C. Simo, R. L. Taylor, and K. S. Pister. Variational and projection methods for the volume constraint in finite deformation elasto-plasticity. *Computer Methods in Applied Mechanics and Engineering*, **51**:177–208, 1985.

[56] Paul Steinmann and Erwin Stein. On the numerical treatment and analysis of finite deformation ductile single crystal plasticity. *Computer Methods in Applied Mechanics and Engineering*, **129**(3):235–254, January 1996.

[57] D. Sulsky, Z. Chen, and H. L. Schreyer. A particle method for history-dependent materials. *Computer Methods in Applied Mechanics and Engineering*, **118**:179–196, 1994.

[58] D. Sulsky and A. Kaul. Implicit dynamics in the material-point method. *Computer Methods in Applied Mechanics and Engineering*, **193**:1137–1170, 2004.

[59] D. Sulsky and H. L. Schreyer. Axisymmetric form of the material point method with applications to upsetting and Taylor impact problems. *Computer Methods in Applied Mechanics and Engineering*, **139**:409–429, 1996.

[60] D. Sulsky, S.-J. Zhou, and H. L. Schreyer. Application of a particle-in-cell method to solid mechanics. *Computer Physics Communications*, **87**:236–252, 1995.

[61] Geoffrey Taylor. The use of flat-ended projectiles for determining dynamic yield stress. I. Theoretical considerations. *Proceedings of the Royal Society of London, Series A, Mathematical and Physical Sciences*, **194**(1038):289–299, September 1948.

[62] Gustavo Weber and Lallit Anand. Finite deformation constitutive equations and a time integration procedure for isotropic, hyperelastic-viscoplastic solids. *Computer Methods in Applied Mechanics and Engineering*, **79**(2):173–202, March 1990.

[63] Z. Wieckowski. The material point method in large strain engineering problems. *Computer Methods in Applied Mechanics and Engineering*, **193**(39-41):4417–4438, October 2004.

[64] Mark L. Wilkins and Michael W. Guinan. Impact of cylinders on a rigid boundary. *Journal of Applied Physics*, **44**(3):1200–1206, March 1973.

[65] Heng Xiao and Liang-Sen Chen. Hencky's logarithmic strain and dual stress-strain and strain-stress relations in isotropic finite hyperelasticity. *International Journal of Solids and Structures*, **40**(6):1455–1463, March 2003.

[66] O. C. Zienkiewicz and R. L. Taylor. *The Finite Element Method*, volume 2: Solid mechanics. Butterworth-Heinemann, Boston, 5th edition, September 2000.

A Alternative implementations of the mixed formulation

Equations (88d) - (88e) are not necessarily the only way to update the element level mixed volume. As alternatives, the following two options are possible:

1. Incremental multiplicative update:

$$\sum_{pt=1}^{N_{pt}} \delta p^h(\boldsymbol{\varphi}_n^{pt}) \cdot \left[\theta^h(\boldsymbol{\varphi}_n^{pt}) \cdot J_n^{pt} - J_{n+1}^{pt}\right] \ \Omega_0^{pt} = 0, \tag{108a}$$

$$\Theta_{n+1}^{pt} = \theta^h(\boldsymbol{\varphi}_n^{pt}) \cdot \Theta_n^{pt}. \tag{108b}$$

   For this update method, an estimate of

$$\sum_{pt=1}^{N_{pt}} \delta p^h(\boldsymbol{\varphi}_n^{pt}) \cdot \left[\Delta\Theta^{pt} - \Delta J^{pt}\right] \ \Omega_0^{pt}$$

   cannot be easily computed. Thus it is not possible to verify the energy conservation properties (or lack thereof) of this update scheme.

2. Total Lagrangian update:

$$\sum_{pt=1}^{N_{pt}} \delta p^h(\boldsymbol{\varphi}_n^{pt}) \cdot \left[\theta_{n+\alpha}^h(\boldsymbol{\varphi}_n^{pt}) - \det(\mathbf{F}_{n+\alpha}^{pt})\right] \ \Omega_0^{pt} = 0, \tag{109a}$$

$$\Theta_{n+\alpha}^{pt} = \theta_{n+\alpha}^h(\boldsymbol{\varphi}_n^{pt}) \tag{109b}$$

   for all $\alpha \in [0,1]$. In this case there is no need to store Θ at the material points. The average volumes $\{\Theta_n, \Theta_{n+1}\}$ are computed directly. In this case, the values of Θ_n and Θ_{n+1} change during the regrid step(4) of Algorithm MPM since the pressure/volume interpolation changes. The pressure/volume interpolation is grid based, and when particles move to neighboring elements the mixed volume in those elements changes. Thus the values of $U(\Theta^{pt})$ change, and the energy conservation properties of this update scheme are unknown.

Since it is not possible to evaluate the energy conservation properties of these alternatives, the additive update (88d) - (88e) is chosen for this work. However, *all three options are equivalent for a Lagrangian Q1/P0 finite element simulation.*